INSTITUTE FOR AEROSPACE STUDIES

UNIVERSITY OF TORONTO

AN EXPERIMENTAL INVESTIGATION INTO THE SHAPE OF THRUS AUGMENTING SURFACES IN CONJUNCTION WITH COANDA-DEFLEC JET SHEETS (PART II)

by

T. Mehus

UTIAS

JANUARY, 1965 UTIAS TECHNICAL NOTE NO. 7

AN EXPERIMENTAL INVESTIGATION INTO THE SHAPE OF THRUST AUGMENTING SURFACES IN CONJUNCTION WITH COANDA-DEFLECTED JET SHEETS (PART II)

by

T. Mehus

JANUARY, 1965

UTIAS TECHNICAL NOTE NO. 79

ACKNOWLEDGEMENTS

The author wishes to express his sincere thanks to Dr. G. N. Patterson for the opportunity to pursue this research.

The author is also indepted to Dr. G. K. Korbacher for his helpful advice and supervision of this project. Special thanks are due to Professor B. Etkin for his valuable supervision in the absence of Dr. Korbacher. Useful discussions with Messrs. D. Whittley and D. Garland, DeHavilland Aircraft Co. of Canada Ltd. are much appreciated. The assistance of Messrs. C. D. Hope-Gill and Y. Nishimura with the experimental work is also gratefully acknowledged.

This work was made possible through the financial assistance of the U. S. Army/TRECOM, Grant DA TC-44-177-G1, Task 1D121401A14224.

SUMMARY

The present work is a continuation of the experimental investigations described in Part I. The subject was to increase the thrust augmentation of a configuration consisting of a Coanda surface (quadrant), deflecting the primary jet sheet through 90°, in conjunction with additional (thrust augmenting) surfaces. The effect of a horizontal and vertical gap between the lip of the nozzle and the leading edge of the deflection surface, as well as the effect of a gap between its trailing edge and the downstream diffuser wall (tertiary flow) was studied. These experiments were carried out for a convergent (subsonic) and a convergent-divergent (supersonic) nozzle at various pressure ratios. The subsonic jet sheet produced the highest thrust augmentation. Tilting of the quadrant led to an increase in the augmentation ratio (excluding the lift acting on the nozzle), while the total thrust augmentation (including the lift over the nozzle) did not increase. Typical secondary and exit mixed flow velocity profiles were obtained. The highest total thrust augmentation observed was 1.37.

TABLE OF CONTENTS

NOTATION

L	measured lift or vertical force on the entire suspended thrust augmenting rig, lbs.
D	measured drag or horizontal force on the entire suspended thrust augmenting rig, lbs.
L_F	measured lift or vertical force on the external three flaps (augmenting surfaces), lbs.
D_F	measured drag or horizontal force on the external three flaps, lbs.
L_N	estimated lift or vertical force on the nozzle surfaces, lbs.
D_N	estimated drag or horizontal force on the nozzle surfaces, lbs.
L_T	total lift = $L + L_N$, lbs.
D_T	total drag = $D + D_N$, lbs.
TH	thrust, lbs.
F	impulse function (lbs.)
J	momentum flux, lbs.
P	pressure
R	radius of Coanda surface or deflection surface
L. E.	leading edge of deflection surface
T. E.	trailing edge of deflection surface
H	length of the interior flap
d	width of the diffuser inlet
ℓ	horizontal distance between nozzle lip and leading edge of deflection surface
a	vertical distance between nozzle lip and leading edge of deflection surface
t	throat height of two-dimensional nozzle

A	area
P.R.	pressure ratio = P_o/P_a
M	Mach No.
m	mass flow, slugs/sec
V	velocity, ft/sec
T	temperature, ^oR
ρ	density, slug/ft^3
α	angle between the horizontal and the tangent to the lip of the top exterior flap originating from L.E.
β	the angle of the top exterior flap from its vertical position
γ	the angle of the bottom exterior flap from its vertical position
φ	the angle of the interior flap from the vertical
ε	initial angle of deflection surface
ϕ	thrust augmentation = L/J_1
ϕ_T	total thrust augmentation = L_T/J_1
μ	mass augmentation = m_3/m_1

Subscripts

1	exit plane of primary jet
2U	inlet plane of upper secondary flow
2L	inlet plane of lower secondary flow
3	exit plane of mixing channel or diffuser
a	ambient or atmospheric conditions
o	total head or reservoir conditions
m	maximum thrust augmentation (ϕ) at certain configuration
s	control surface
c	conditions of the Coanda (deflection) surface

I. INTRODUCTION

It has been well established through experiments that a jet sheet can be turned efficiently by a multiple-flat-plate or smoothly curved deflection surface through a wide range of turning angles. This phenomenon, known as the Coanda effect (named after its discoverer), is due to the resulting pressure difference across the jet sheet. It also applies whether the deflection surface is attached to or detached from the nozzle, as long as the gap does not exceed that which causes the flow to separate from the surface.

Defining the turning efficiency of the jet sheet as the ratio η of the measured vertical lift on the deflection surface to the ideal thrust of the horizontal nozzle, it was found in the experiments described in Refs. 1 and 2 that high values of η were obtained for both subsonic and supersonic jet sheets. In those experiments the deflection surface was detached from the nozzle for practical reasons, but the gap was kept at an absolute minimum. Korbacher (Ref. 3) found that by widening both the horizontal and vertical gap, an increase in η resulted, with $\eta_{max} = 0.96$ for a 90° deflected jet sheet at pressure ratios above 2.0.

The logical next step was then to try to increase η above unity (thrust augmentation). It is of course not essential to turn the flow in order to obtain augmentation of the thrust, but by doing so, one takes advantage of the better entrainment properties of a curved jet sheet as compared to a straight one. Besides, curved jet sheets can be very useful in, for example, V/STOL-vehicles.

The whole concept of thrust augmentation rests upon entrainment of air, and the degree of augmentation depends on both the relative amount of entrained (secondary) mass flow and on how efficiently this flow is mixed with the primary mass flow; that is to say, the amount of viscous losses which are experienced during the mixing process.

Thrust augmentation can be obtained by arranging a suitable shroud around the primary jet, thereby creating a boundary for the mixing as well as a suitably oriented inlet channel for the secondary flow and outlet channel (diffuser) for the mixed flow.

A quantitative theoretical prediction of the degree of augmentation is difficult, if not impossible, for a number of reasons, the main one being the lack of a complete understanding of the mixing process and consequently the establishment of the equations governing this process. Another complication as encountered in a strict analysis is the unpredictable interactions of several parameters. For instance, by altering one test parameter and thereby improving the flow picture in one respect, it might very well be that an adverse effect on the overall augmentation ratio results. For this reason experimental investigations into factors affecting the augmentation of the thrust are essential and needed.

This work is a confirmation of the experimental investigation carried out by Hope-Gill (Ref. 4) in Part I of this study.

II. TEST FACILITIES AND EQUIPMENT

2.1 General Description

The test equipment used in this investigation was basically the same as described in Part I (Ref. 4). The major difference was the additional use of a two-dimensional convergent-divergent nozzle and of some surfaces employed at a tertiary flow inlet. The general arrangement and some details are shown in Figs. 1 and 2. A brief description follows.

2.2 Air Supply

Compressed air was suppled from a Turbomeca Palouste 500 Gas Turbine. According to Ref. 5, this unit is capable of supplying 2.7 pounds of air per second at a pressure ratio 3.8:1. The compressed air was ducted to the settling chamber of the Coanda test rig by means of eight inch diameter piping after passing through a large water cooler which reduced the air temperature from up to 450°F to approximately 60°F.

2.3 The Nozzles

The interchangeable rectangular subsonic and supersonic nozzles were installed by bolting them to the flanged end of a bellmouth or contraction section mounted in the end of the settling chamber. In order to reduce the blockage effect on the secondary flow from the cylindrical settling chamber, the nozzles were made 7 inches long. The nominal throat area of both nozzles was 1 in^2 (8" x 1/8"), giving a jet sheet aspect ratio of 64.

The supersonic nozzle was designed for an exit Mach number of 1.3 (pressure ratio of 2.77). In order to find the actual Mach number, six static pressure tabs were mounted flush at the exit, three each on the upper and lower lip. As they all were connected to a water manometer through a common tube, an average exit static pressure ($\bar{P}_1$) was obtained.

2.4 The Test Rig

This consisted of the Coanda (deflection) surface, the interior flap hinged to its T.E. and the three exterior flaps. The deflection surface was a quadrant (R = 4") of the same widths as the nozzle exit (8"). The leading edge of the quadrant was extended by a 1/4" flat surface, and the quadrant could be rotated (or tilted) about an axis located some distance away from its center. The three exterior flaps were hinged together and supported solely by a frame connected to a strain gauge system mounted rigidly to the frame of the thrust augmenting rig.

The quadrant and the flaps (but not the nozzle) were enclosed by glass sidewalls on either side in order to simulate two-dimensional flow. A pit below the mixing channel exit was designed so that any ground effect was eliminated. The weight of the entire rig was suspended primarily by a balance with a fixed fulcrum and the Coanda quadrant plus support was suspended by another strain gauge balance situated below the settling chamber.

The variables of the test rig are shown in Fig. 2. The entire rig could be adjusted horizontally and vertically, providing various gap sizes defined by the distances ℓ and a. All the flap angles could be varied by means of the connecting rods. The choice of relating α to the L. E. instead of to the fixed nozzle lip was based on practical considerations, and is in line with the definition used in Part I.

Unfortunately, there were some mechanical limitations on the rig. In order to avoid any part of the balanced rig to touch the fixed nozzle, the smallest obtainable ℓ was restricted by the glass-plates hitting the nozzle lip. The flange under the nozzle (see Fig. 1) restricted the tilting angle ε and also the vertical gap size a. Thus at $\varepsilon_{max} = 12^o$, $(\ell/t)_{min} = 1$ and $(a/t)_{min} = 5.6$.

2.5 Instrumentation

The linkages of both strain gauge balance systems allowed the mutual perpendicular components of the lift and drag forces to be measured independently of each other. The strain associated with these forces were measured on two separate SR-4 Strain Indicators (type N), and the actual forces was obtained directly from the calibration curves of the balances. The indicator connected to the main balance measured the vertical force (L) and the horizontal force (D) on the entire suspended rig, while the other indicator measured merely the vertical (L_F) and horizontal (D_F) forces acting on the three exterior flaps. All the strain gauge electrical bridge network was arranged so that strain gauges were self-compensating with respect to external temperature changes.

The static pressure on the upper nozzle surface was measured with a probe held parallel to the flow and close to the surface. The same static pressure probe was employed across the lower secondary flow inlet, $A2_L$ (see Fig. 3), while a rake was used across the upper secondary flow inlet ($A2_U$) and at the exit of the mixed flow (A_3). The total head across A_3 was measured with a single total pressure probe. All these probes were connected to a water manometer.

The primary mass flow was measured by means of an orifice type meter (Ref. 6) situated in the pipe downstream of the water cooler. A U-tube water manometer recorded the pressure difference across the orifice plate. The total pressure of the primary air was measured by a mercury manometer connected to a pressure probe located in the settling chamber.

The primary flow temperature was measured with a standard glass thermometer located just downstream of the cooler. The engine and airbleeding controls were centrally located, away from the sound-isolated engine room.

3. THEORETICAL REMARKS

3.1 Introductory Comments

If by thrust augmentation one means the ratio of the total thrust acting on a system to the thrust of the primary flow, it is obvious that one has to strive for the highest possible total outlet momentum from the system in order to get maximum augmentation. This means a large mass flow and/or velocity of the exit of the mixing channel diffuser.

As stated in Ref. 7, a thrust augmenting device is in effect an ejector in which the emphasis is laid on an increase in the momentum rather than on either mass augmentation or "jet pump" (pressure rise) capabilities. Further, in general, thrust augmentation depends on the geometry of the ejector, the flow properties of the primary and secondary flows and the exit conditions at the end of the mixing channel.

3.2 Momentum Box Theory

Consider a stationary thrust augmenting device as shown in Fig. 4. The arrangement shown is essentially the same as that which was used in this experiment. The chosen control surface, indicated by the broken line(s), may be considered approaching infinity.

The entrainment of secondary air might be considered as a sink effect at the inlet. By continuity, the resulting induced velocity, V_i, across the control surface, s, varies inversely with s, i.e. $V_i \propto 1/s$. It follows that for the control surface area approaching infinity, the flow velocity across s will become infinitly small, and all terms containing V_i^2 will vanish like $1/s^2$. Thus the momentum terms at the control surface, in both the horizontal and vertical direction of the entrained flow, are of the order

$$\lim_{s \to \infty} \int \rho\, V_i^2\, ds = \text{const.} \lim_{s \to \infty} \int \frac{ds}{s^2} = 0$$

and consequently, the static pressure of the control surface (except over A_1 and A_3) is

$$P = P_\infty \to P_a \quad \text{as } s \to \infty \, .$$

Hence, there is no pressure difference across the control surface and the total momentum approaches zero. In practice it was observed that only a relatively short distance away from the "sink", it was impossible to indicate any difference between the static pressure and P_a with the static pressure probe.

If the primary momentum flux enters the system horizontally and the mixed flow momentum flux leaves it vertically, by applying the momentum theorem, the vertical reaction force on the system simply becomes

$$R_y = \int \rho V_3^2 \, dA + (P_3 - P_a) A_3 = F_3$$

and the horizontal reaction force

$$R_x = +\int \rho_1 V_1^2 \, dA + (P_1 - P_a) A_1 = F_1$$

From these relations it is seen that the inlet momentum of the secondary flow does not have to enter explicitly into the analysis of R_y and R_x.

3.3 The Reaction Forces

These are the forces acting on the surfaces in the control box due to pressure and friction induced by the flow passing over them. They include the forces on the Coanda quadrants, the flaps, and on the nozzle itself as well as on any other structural surfaces in the flow field.

These forces are the lift and drag (L_c and D_c) on the Coanda surface (including the forces on the interior flap and the quadrant's supporting structure), the lift and drag on the exterior flaps (L_F and D_F), and the lift and drag on the nozzle (L_N and D_N). The latter forces have to be estimated from static pressure measurements over the fixed nozzle, and the net lift on the nozzle is the sum of the lift on the top surface (L_{NT}) and the lift on the bottom surface of the nozzle (L_{NB}); i.e., $L_N = L_{NT} + L_{NB}$. The other forces are included in the measured (balance) forces L and D, i.e. $L = L_c + L_F$, $D = D_c + D_F$. The total lift on the surface is

$$L_T = L + L_N = R_y = F_3$$

and the total drag is

$$D_T = D + D_N = R_x = F_1 \; .$$

Assuming that $P_1 = P_3 = P_a$, the total lift and drag reduce to

$$L_T = J_3 \text{ and } D_T = J_1 \; .$$

3.4 The Lift on the Coanda Surface

The largest contribution to the total lift naturally comes from the lift over the deflection surface where the flow velocities are highest. In the ideal case of non-viscous flow, the jet sheet would attach to the curved surface with constant thickness (= t) as long as there exists radial equilibrium between the centrifugal force and the pressure force acting on

the jet sheet. Considering an element of the sheet (see, for example, Ref. 3) one finds that

$$\Delta P = P_s - P_c = \rho_1 t \cdot \frac{V_1^2}{R} ,$$

where P_s is the static pressure on the free surface of the jet sheet and P_c is the static pressure at the Coanda surface. For incompressible flow, Bernoulli's equation would apply along any streamline of the secondary flow, and

$$P_a - P_s = \tfrac{1}{2} \rho \cdot V_s^2 .$$

Assuming atmospheric pressure beneath and no tilting of the quadrant, the lift on the Coanda surface alone is (as in Ref. 4)

$$L_c = R\,(P_a - P_c) = R(P_a - P_s + \Delta P) ;$$

therefore

$$L_c = \rho_1 t V_1^2 + \tfrac{1}{2} \rho\, R V_s^2 .$$

(For compressible flow, a correction for this would have to be added.)

Therefore, for a given Coanda surface and primary jet, an increase in the lift on the deflection surface can only be obtained by increasing V_s (or decreasing P_s). This means that the pressure on the Coanda surface (P_c) must adjust itself correspondingly to a lower pressure in order to keep ΔP constant. The velocity V_s can be increased by promoting entrainment, whereby the velocity of the entrained (secondary) air across the entire inlet is increased. The prime function of the upper portion of the thrust-augmenting surface is to do this by providing a suitable convergent entrance channel for better mixing of the secondary flow with the primary jet sheet.

3.5 Mixing

One might consider the mixing of the primary and secondary air as taking place in two regions (see Fig. 3). The first one can be referred to as the primary mixing zone. It extends over that portion of the curved jet sheet, which is occupied by the potential mixing cone. In this region the thickness of the jet sheet is gradually increased from its original value of t. Beginning where the primary mixing zone ends, a secondary mixing zone may be defined. In this region the thickened curved jet sheet mixes with the remaining part of the secondary mass flow. Mixing in both regions has to be optimized through a suitably shaped mixing channel, the desired end result being a most uniform exit velocity (V_3).

By forcing or guiding the entrained (secondary) mass flow into a direction more or less parallel to the primary mass flow, the mixing properties will most likely be favourably changed. Consider the unshrouded and the shrouded configuration in Fig. 3. The entrainment may be consider-

ed as a sink effect, and as a result the induced secondary flow velocity will be more normal to the primary velocity direction in the first case than in the second case where, due to the shrouding, the secondary flow has been accelerated parallel to the primary flow.

3.6 Optimum Configuration

As an attempt to clarify the physical relations between the related mixed flow exit momentum and the vertical reaction forces, the following can be said. By decreasing the entrance area A_2 and thereby increasing $\bar{V}_2$, L_c would increase as explained above. But at the same time the suction or reaction forces on the flaps and the nozzle might change in such a way that they more or less cancel the gain in L_c, depending on the chosen configuration.

Correspondingly, an increase in $\bar{V}_2$ may at first seem only desirable since $J_3 \propto J_2$; but if A_2 (and the diffuser width) is made too small, it might have an adverse effect on the entrainment and on the mixing properties, actually resulting in a smaller J_3. Whether one considers an increase in thrust augmentation as a result of either a larger L_T or a larger J_3, it seems obvious that there must exist one or more optimum configurations. Furthermore, whatever the effect upon the mixing might be, by providing an entrance channel, more useful momentum can be "picked up" in this case as compared with the use of no shrouding.

From the above discussion, it can be concluded that the magnitude of the secondary air inlet momentum flux ($\int \rho \ V_2^2 \ dA$) plays a definite role in thrust augmentation, while its direction may or may not be important, depending on the resulting reaction forces acting on the surfaces. But the total lift L_T ($\propto$ thrust augmentation) is equal to F_3 regardless of what the total inlet momentum, F_2, may be. This follows from the fact that all entrained air is originally at rest at infinity (stationary system, see Ref. 8).

3.7 Theoretical Prediction of Thrust Augmentation

So far the origin of thrust augmentation has been treated only from a qualitative viewpoint. In Refs. 7 and 8, where geometrically simpler models were employed, the thrust augmentation is predicted analytically after assumptions are made regarding velocity distributions, pressures, etc. In Ref. 8 it is shown that the thrust augmentation in the case of a nonuniform secondary velocity distribution can be considerably larger than in the case of a uniform distribution. In Ref. 7 it is stated that large thrust augmentation can be obtained with a large value of $(V_2/V_1)^2$, both for constant pressure mixing and constant area mixing, for incompressible flow and compressible flow. Since the thrust augmentation depends on the square of the secondary velocity, it is suggested in Ref. 7 that one should perhaps choose a value of the area ratio A_2/A_1 smaller than that which is conventional for mass aug-

mentors. On the basis of this and the discussions in the previous section, it seems reasonable to believe that it is desirable, in general, to have a high V_2/V_1 ratio.

In order to predict the thrust augmentation of a system, one has to find an expression for the total exit momentum of the mixed flow in terms of known quantities. Consider the two-dimension device in Fig. 4, but for simplicity with no gap between the quadrant L.E. and the nozzle. If one considers the flow through a section across the primary and secondary inlets and through a section across the exit of the mixing channel, one can apply the momentum equation in the x- and y-direction and the continuity equation. The quantities involved in these three equations are ρ , A, V, and P, and since the walls are not parallel, the reaction forces R_x and R_y do enter the momentum equation as well. For a given geometrical configuration, all the areas are known; and for a given pressure ratio also V_1 and ρ_1 are known. For the case of incompressible flow, P_2 is given in terms of V_2 (Bernoulli) and $\rho_2 = \rho_3 = \rho_a$. One may also assume that $P_1 = P_3 = P_a$.

Even if one further assumes a certain velocity distribution of the flow at the two cross sections A_2 and A_3 (which in itself may be difficult), it is seen that one is left with four unknowns, (V_2, V_3, R_x and R_y) and only three equations. (Of course the terms which include V would have to be integrated across the respective sections.) Allowing for additional entrainment, as for example through a gap between the nozzle and the L.E., would complicate the analysis further. The mixing equation, or equations, are obviously the ones which represent and describe the flow mixing process (or processes), the rate and degree of momentum and energy transfer between the two flows for the given conditions.

For such an arbitrary thrust-augmenting device, it therefore seems impossible to predict theoretically the thrust augmentation with the present lack of a complete understanding of the mixing process.

4. THE OBJECT OF THIS STUDY

The object of this experimental investigation was to find out more about the shape of thrust-augmenting surfaces for optimum augmentation in conjunction with Coanda deflected jet sheets. Also the effect of tilting the Coanda block and its position relative to the nozzle lip was to be investigated. All this was done for both subsonic and supersonic jet sheets.

4.1 Part I and Its Findings

In Part I (Ref. 4) the quadrant was kept in a fixed untilted position relative to the lip of the nozzle, the gap being so small that any entrainment through it could be neglected. The effect upon ϕ of the position of the upper flap forming the inlet channel was investigated as well as the

shape of the mixing channel. Only the convergent nozzle was employed, but three quadrants of various radii were tested.

In summarizing some of the main findings, it was found that several optimum configurations yielded a maximum total thrust augmentation (ϕ_T) of 1.21. There was no significant change in $(\phi_T)_m$ by varying the pressure ratio between 1.1 and 1.5, but above this value, a slight decrease was observed. While ϕ_T was found to be practically independent of R, it appeared to be a linear relationship between ($\alpha - \beta$) and R, which yielded optimum augmentations. The optimum shape of the mixing channel was given by a length to width ratio of $(d/H) \approx 6$, and a total enclosed diffuser angle of about 6°.

4.2 Part II and Its Objectives

In the present work the effect of an additional secondary flow inlet between the nozzle lip and the L.E. of the deflection surface (see A_{2_L} in Fig. 3) as well as the effect of a tertiary flow between its T.E. and the interior flap was investigated. Furthermore, the effect of tilting the quadrant and variation of the diffuser angle at the same time was investigated. Also the effects of a rounded L.E. on the deflection surface was explored. These runs were carried out with both the convergent nozzle (employed in Part I) and a new convergent-divergent nozzle (with the same nominal throat dimensions) at several pressure ratios.

4.3 Basic Test Configuration

In light of the many possible test parameters involved, a basic shape of the exterior flaps had to be chosen, based on the findings of Part I. For the four inch quadrant, the optimum ($\alpha - \beta$) was found to be near 20°. A slight decrease of ϕ_T was observed when $\beta > 20^{\circ}$, possibly caused by the resulting poorer inlet channel. The optimum d/t-ratio was found to be independent of R and was approximately 26 at a pressure ratio of 1.5, increasing only slightly with increasing pressure ratio.

On the basis of this, the following basic flap configuration was chosen for Part II:

$$R = 4''$$
$$\alpha = 40^{\circ}$$
$$\beta = 20^{\circ}$$
$$\gamma = 6^{\circ}$$
$$\varphi = 0^{\circ}$$
$$d/t = 26.4$$
$$H/d = 6$$

However, a series of runs was performed with $\alpha = 60^{\circ}$, $\beta = 40^{\circ}$, all the other parameters unchanged.

The middle exterior flap was kept vertical at all times, and with $\beta = 20^{o}$, the flexible metal sheet attached tangentially to the top and middle flap, formed a reasonably convergent inlet.

5. TEST PROCEDURE

Before each test run, the L.E. of the quadrant was set at the required position and the zero readings on both strain gauge indicators were taken. Then, the air bleed valve was opened and the desired pressure ratio (based on temperature corrected atmospheric pressure) was set. Due to the load on the rig, readjustments were then required on the deflection surface in order to bring it back to its correct position relative to the nozzle exit. This was mainly a small adjustment of the vertical distance (a), and at a given ℓ, it did not affect the zero readings. When the whole system had attained equilibrium, the following data were taken:

1) the strain gauge balance readings

2) the primary air flow temperature and

3) the differential head of the primary mass flow.

With the supersonic nozzle, the exit pressure $\bar{P}_1$ was recorded in addition. As this nozzle was employed at P.R. = 1.5, 2.0 and 2.77, testing time was saved by using the same zero balance readings for all three pressure ratios. In other words, for a given configuration, the readings for the three pressure ratios were taken successively by just altering the engine controls and readjusting a for each pressure ratio.

The subsonic nozzle was only tested at P.R. = 1.5 and the tertiary flow experiments were merely performed at this pressure ratio.

The test range of the horizontal and vertical gap with the untilted quadrant was $1 < \ell/t < 8$ and $0.8 < a/t < 6.4$. The test range of ε (tilting) was from 0° to 12°, but as ε increased, the possible range of ℓ and a decreased.

Each time the quadrant was rotated to a new ε value, the three exterior flaps had to be reset in order to maintain the basic test configuration described in section 4.3.

The pressure distributions over the nozzle surfaces, as well as across the secondary inlet and mixed flow exit areas were recorded for several near optimum configurations.

It was observed that daily variations in the atmospheric conditions could have a small effect upon the consistency of the test results. Therefore, when ever possible, a test series was started and completed on the same day.

6. RESULTS AND DISCUSSION

6.1 Definition of Thrust Augmentation

The definition of thrust augmentation, ϕ, used in this report is based on the ratio of the measured lift, L (lbs), on the entire rig (excluding the lift L_N over the nozzle) to the primary nozzle momentum flux, $J_1 = m_1 V_1$ or

$$\phi = \frac{L}{J_1} = \frac{L}{m_1 \sqrt{\frac{2\,k\,R\,T_o}{k-1}\left[\frac{(P_o/P_a)^{k-1/k} - 1}{(P_o/P_a)^{k-1/k}}\right]}} .$$

Here, m_1 is the measured primary mass flow and V_1 is the theoretical primary nozzle exit velocity computed by the above square root expression. Thus, by this definition, the vertical lift (thrust) on the system is compared with the thrust of this particular nozzle if the primary flow would expand isentropically.

In a few cases, the lift L_N over the nozzle was calculated and added to the balance measured lift. In these cases, the total thrust augmentation of the entire system is defined as

$$\phi_T = \frac{L_T}{J_1} = \frac{L + L_N}{J_1}$$

6.2 Primary Momentum Flux Used in the Calculation of ϕ

The following values of J_1 are used in this report: (see Appendix for details). At a pressure ratio of 1.5 for both the subsonic and supersonic nozzle J_1 = 12.02 lbs. For the supersonic nozzle, J_1 = 21.6 and 36.75 lbs at pressure ratio 2.0 and 2.77 respectively.

6.3 Reduction and Presentation of the Test Results

The measured units on the strain gauge indicators were divided by the respective calibration factors in order to obtain the actual forces L, D, L_F and D_F in pounds. Then these were non-dimensionalised by dividing by J_1.

The bulk of the experimental results is presented as a plot of ϕ and D/J_1 versus a/t and ℓ/t at the various pressure ratios and ε. Also L/D is plotted vs. a/t for some ℓ/t ratios, mostly for a qualitative comparison with the ϕ-curves.

Unless otherwise stated on the figures, they all correspond to the basic flap configuration as listed in section 4.3.

6.4 Results with the Subsonic Nozzle

6.4.1 Effect of Vertical Gap (a) on ϕ

Figure 5 shows that ϕ increases almost linearly with a/t until an optimum value of ϕ is reached. With a further increase in a/t, ϕ seems to stay rather constant, followed by a slight decrease as (a) approaches its mechanically possible maximum value. A further increase in (a) would have been too risky anyway as the jet sheet was believed to be close to separation.

Because of the inherent growth in thickness of the jet sheet due to entrainment, the actual vertical gap between the jet sheet and the Coanda surface decreases with increasing ℓ . Hence the "safe" (safe against separation) nominal vertical gap size is smaller at small ℓ than at larger ℓ values and a_{min} is defined as that gap at which the jet sheet is just hitting the L. E. of the deflection surface. This explains why for optimum ϕ , both a/t and ℓ/t have to be relatedly increased as shown in Figs. 5 and 6. It also explains why the optimum a/t seems to be smaller at small ℓ/t values than at large ℓ/t values.

In Fig. 6 the results are plotted for a similar configuration as in Fig. 5, the only difference being the increase in α and β to 60° and 40° respectively (ε = 0° in both cases). The trend is the same in both figures even though the ϕ -curves are less linear in Fig. 6 and indicate a maximum of ℓ/t = 8 rather than at ℓ/t = 3 as in Fig. 5. However, ϕ at a/t = 5.6 (Fig. 6) differs little with ℓ/t. The maximum thrust augmentation, ϕ_m in Fig. 5 (α = 40°, β = 20°) was ϕ_m = 1.452 at ℓ/t = 3 and a/t ≈ 5.5, while in Fig. 6 (α = 60°, β = 40°) reduces to ϕ_m = 1.42 at ℓ/t = 8 and a/t ≈ 5.5. These observations agree with the findings in Part 1 (Fig. 34) which indicate for the case of a negligible a/t that the augmentation is practically unchanged for these two configurations. The slightly higher ϕ_m in case 1 was the reason why this configuration was used throughout the present experiments.

It was found, as in Part I, that case 2 yielded a slightly higher lift over the nozzle because the upper secondary airflow was more parallel to the nozzle axis.

6.4.2 Effect of Horizontal Gap (ℓ) on ϕ

This effect is partly illustrated in Fig. 5; but it is shown best in Fig. 7, where the maximum ϕ -values (taken from the various ℓ/t-curves in Fig. 5) are plotted versus ℓ/t. Figure 7 shows that for ε = 0°, the optimum value of ℓ is about 3 to 4 times the nominal throat height. Unfortunately (for mechanical reasons), the only position of the quadrant at which the entire range of ℓ/t could be investigated was at ε = 0°. The ε = 0° curve is rather flat; and since it gives the variation

of ϕ_m with ℓ/t for an almost constant a/t value (= 4.5 ÷ 5.5), it can be compared with the curves in Fig. 5 for constant ℓ/t-values. Such a comparison indicates that the vertical gap has a much stronger effect on ϕ than the horizontal gap, in that the variation in ϕ over the entire ℓ/t range was only about half that which resulted from the variation in a. However, the effect of ℓ seems to become more pronounced as ε is increased (see, for example Fig. 7 for $\varepsilon = 10^o$).

6.4.3 Effect of Tilting the Quadrant (ε) on ϕ

Tilting of the quadrant led to an increase in ϕ . This is illustrated in Figs. 7, 8 and 20. The maximum thrust augmentation observed was at $\varepsilon = 10^o$, where $\phi_m \simeq 1.545$. Increasing ε from 0° to 10° resulted in an increase of ϕ , given by $\Delta\phi$ (= 1.545 - 1.27) = 0.275 or 21.6%. This was obtained at a total enclosed diffuser angle ($\varphi + \gamma$) of about 8° but at slightly different a/t and ℓ/t values for $\varepsilon = 0^o$ and $\varepsilon = 10^o$ (see Fig. 8).

The test results with the tilted quadrant (Fig. 7) showed the same trends as those with the untilted quadrant. In other words, by decreasing ℓ from its maximum possible value, ϕ increases initially. The dotted lines on Fig. 7 indicate the expected dependence of ϕ and ℓ which most likely exists at ℓ -values smaller than those which could actually be obtained on this rig.

6.4.4 Effect of Diffuser Angle on ϕ

The angle γ was kept constant at 6° while φ was varied between 0° and 6° at various angles of tilt of the quadrant. At moderate degrees of ε , the augmentation ratio was found to decrease with φ (Fig. 8). The rate of decrease becomes smaller with increasing tilt angle. From about $\varepsilon = 6^o$ and larger, a considerable increase in ϕ was observed when the interior flap angle φ was increased to about 2°, but ϕ decreased again with larger φ -values (see Fig. 8). In conclusion, at $0^o \leq \varepsilon < 6^o$, the optimum enclosed diffuser angle ($\varphi + \gamma$) was about 6°, while at $6^o < \varepsilon < 12^o$, ($\varphi + \gamma$) was about 8°. A combination of $\varphi = 4^o$, $\gamma = 4^o$ (at large ε) caused practically no change in ϕ in most cases, but with $\gamma = 2^o$, $\varphi = 6^o$, there was a decrease. Wool-tufts indicated that separation along the interior flap occured at this value of $\varphi = 6^o$.

The relation between φ , ε and ϕ indicates that the primary (and mixed flow) possibly was turned a bit more fully vertical by increasing ε , thereby increasing ϕ and allowing a more symmetrical diffuser with respect to the vertical.

Again, the variation in ϕ with ℓ is reflected by the two curves at $\varepsilon = 8^o$ in Fig. 8, where obviously the lower ℓ/t-value (closer to the optimum) yields a higher ϕ . For the same reason, the curve for

ε = 12° (at ℓ/t = 8) would most likely lie above the ε = 10° curve if ℓ/t could have been kept at 6.25 also for ε = 12° (see Fig. 7).

No attempt was made to change the length (H) of the diffuser. The diffuser length to width ratio (H/d) was at all times kept at about 6, which was found in Part I to be the optimum value. This figure is the same as obtained in the work described in Ref. 9.

6.4.5 <u>Effect of Tertiary Flow</u>

In order to investigate the effect of a tertiary flow through a gap between the T.E. of the deflection surface and the interior flap on thrust augmentation, a series of tests was conducted for several different configurations, of this opening, some of which are shown in Fig. 26. Different shapes of the curved inlet surfaces were tried in conjunction with variations of the gap (b), the step (c) and the angle φ. These runs were carried out with ℓ/t = 1 and a/t = 3.2, and the position of the three exterior flaps being the same as in previously discussed tests. Also, a series of tests was carried out at ε = 5° and 8°.

In no case during these runs was there observed any gain in the augmentation ratio compared with the previous runs when the interior flap was hinged directly to the T.E. of the quadrant. Actually, the highest thrust augmentation was observed when the tertiary gap was closed (b = 0), and still it was 4 - 5% lower than with the exterior flap hinged directly to the T.E. By increasing b, a gradual drop in ϕ was observed.

6.5 <u>Results with the Supersonic Nozzle</u>

This nozzle was run at pressure ratios of 1.5, 2.0 and 2.77, the latter being the design P.R. corresponding to a Mach No. of 1.3. The justification for testing also this nozzle at P.R. = 1.5 was to see how it compared with a subsonic nozzle (at same P.R.). In the event a supersonic jet sheet should indicate superiority, it would be of interest to know also how it performs at lower pressure ratios.

At P.R. = 2 and 2.77, some variations were observed in the measured exit static pressure P_1 with a at small vertical gap sizes. This indicates the existence of some interference between the L.E. and the shock system. The average values of P_1 were 3.4", 6" and 2.5" H_2O below P_a for the three pressure ratios respectively. Based on the average P_a = 29.3" Hg, this gives the following Mach numbers:

at	P.R. = 1.5	$M_1 \simeq$ 0.79
	2.0	1.06
	2.77	1.348

The results obtained with the supersonic nozzle are plotted in figures 9 to 20.

6.5.1 Effects of a, ℓ and ε

In short, it can be stated that the effects on thrust augmentation of these test parameters were the same in trend as those observed with the subsonic nozzle. The shape of the ϕ -curves is almost the same for all pressure ratios and angles of ε , any deviations from the "expected shape" being most likely within the experimental accuracy.

The optimum a/t is seen to be about 4 to 5 (as before) and seems to become more pronounced with increasing ε .

These results, however, did not show the dependence of ℓ and ε as clearly as with the subsonic nozzle (Fig. 7). Therefore, in Fig. 19, ϕ is plotted as ℓ/t at constant a/t = 4, and this plot together with the rest of the figures indicates that the optimum ℓ/t-ratio still is at around 3÷4. Figures 15 to 17 show clearest how ϕ decreases with ℓ after the optimum ℓ/t ratio is exceeded. Again, variations of the vertical gap seem to have a greater effect upon ϕ than variations in the horizontal gap (ℓ).

The thrust augmentation increases with ε as shown, for example, in Fig. 20. The optimum value of ε may have been reached at the end of the mechanically possible range of ε , i.e. at ε = 10° to 12°. But when studying this figure, it must be kept in mind that with the present rig it was technically not possible to keep a desired gap (ℓ and a) at all angles ε tested. Therefore, the curve for the subsonic nozzle is probably not that peaky at ε = 10° as shown in Fig. 20, since a value of ℓ/t < 8 at ε = 12° most likely would increase ϕ as indicated in Fig. 7.

6.5.2 Effect of Pressure Ratio (P.R.) on ϕ

Figure 20 also demonstrates that ϕ decreases with increasing P.R. A possible exception from this seems to be for ε = 0°, at which ϕ increases somewhat if the P.R. is increased from 1.5 to 2.0 (see also Figs. 9 and 10). But at P.R. = 2.77, ϕ drops again. At, for instance, the configuration given by ℓ/t = 5.25, a/t = 4.8 and ε = 8° and the supersonic nozzle, the augmentation ratio drops about 3% if P.R. = 1.5 is raised to 2.0, and another 5% if P.R. is increased from 2.0 to 2.77.

Also, a comparison of the ϕ data obtained with the two nozzles at the same P.R. = 1.5 shows that the subsonic nozzle is superior to the supersonic nozzle.

6.6 The Measured Horizontal Force or Drag (D)

The ratio D/J_1 is plotted vs. a/t for various ℓ/t-ratios (Figs. 5, 6 and 9 to 17). The resulting curves are rather flat and the scattering of the test points prevents any rigorous conclusions to be drawn

as to the drag variations with ℓ and a. However, it can be said that the D/J_1 ratio varies from unity (except for a very few cases) by only $\pm$ 5% for all configurations and pressure ratios tested, and whether the jet sheet was supersonic or subsonic.

6.7 The L/D Ratio

According to theory:

$$F_1 = D_T = D + D_N$$
$$F_3 = L_T = L + L_N$$

A systematic comparison of these quantities could not be carried out, as it would have involved too many pressure measurements in finding L_N and D_N.

The seondary flow induces suction forces on the nozzle surfaces which, resulting in D_N and L_N, cannot be neglected in a proper comparison. But such a comparison for the ratios F_3/F_1 and L_T/D_T could only be made for one case (see section 6.1.4).

However, evaluated L/D ratios were plotted for various ℓ/t values in order to compare them with $\phi = L/J_1$. The shape of the L/D curves and the corresponding ϕ -curves are naturally quite similar, since the percentage difference between L/D and L/J_1 was only of the order of $\pm$5% (due to D/J_1, deviating from unity by only $\pm$5%).

6.8 The Forces on the Three Exterior Flaps (L_F and D_F)

These forces are included in the balance measured lift and drag forces (L andD) on the entire rig, but could also be measured separately in order to investigate their contribution to L and D.

A typical and representative set of readings for L_F and D_F are plotted in Figs. 21 and 22 for three different pressure ratios and the supersonic nozzle. In Fig. 21, a/t is kept constant while ℓ/t is varied, whereas the opposite is done in Fig. 22. In both cases the quadrant is tilted by $\varepsilon = 4^o$.

These curves show that there is an optimum value for ℓ/t and a/t also with respect to the lift force on the flaps. The optimum ℓ/t value seems to be around 6 while optimum a/t $\approx$ 4. These are approximately the gap sizes which gave maximum thrust augmentation. This indicates that L and L_F are largest for the same configuration (also at P.R. = 1.5). The external flap lift L_F, except at P.R. = 1.5, was negative in all cases where a/t and ℓ/t were near their optimum values and the quadrant was tilted. This means that with the particular flap configuration used throughout these tests, the suction forces on the inside of the flaps were larger than the suction forces over the rounded lip of the top exterior flap in most all cases.

Although of course L_F increases with pressure ratio, the ratio L_F/J_1 decreases, indicating again the disadvantage of the larger pressure ratios with this particular rig.

The horizontal forces on the flaps (D_F) are always negative, naturally, and varied with a and ℓ more or less in the same way as L_F did. D_F was relatively large, for example at P.R. = 20, a/t = 4, ℓ/t = 6, ε = 4° (Figs. 13 and 21), while $D_F/J_1 \cong -2.1$ and $D/J_1 = +0.985$.

Thus the drag force D_C (positive) acting on the Coanda surface and the interior flap was about one and a half times as large as the drag on the exterior flaps (D_F) since $D = D_C + D_F$. This is due to the strong suction force acting on the interior flaps (at P.R. = 2.0, J_1 = 21.6 lbs.).

6.9 Secondary Flow Around the Nozzle

The measurements of the static pressure acting on the upper and lower surfaces of the nozzle showed that the velocity profiles taken perpendicular to the nozzle axis were quite symmetrical laterally (see Fig. 23). The nonuniform longitudinal distribution was partly due to blockage effects from the settling chamber or the structure under the nozzle and partly due to the glass sidewalls which did not extend beyond the nozzle lip. Thus the air was entrained also from the sides. This particularly applied to the lower surface since a flange almost touched it, preventing a natural inflow.

The static pressure measured along the 1/4-lines differed about 25% from the readings along the midline (at all pressure ratios and configurations) and was found to give a good average value for the pressure distributions on both surfaces. A typical plot of the longitudinal distribution is shown in Fig. 23.

The pressure over the nozzle was measured for a sufficient number of configurations to establish its effect on the total lift. The parameters ℓ, a and ε, were varied one at a time. It was found that L_N

increased with ℓ
decreased with a
decreased with ε

The lift on the top surface (L_{NT}) was practically unaffected by these parameter changes. The variation in pressure or L_{NB} on the bottom surface was a result of varying magnitude and direction (relative to the nozzle surface) of the lower secondary flow. By tilting the quadrant (keeping ℓ and a constant), the lower secondary flow inlet was improved, and the combination of forcing the flow closer to the nozzle and increased mass flow resulted in a higher suction pressure on the bottom surface.

The variation in L_{NB} with a was particularly noticeable at small ℓ/t ratios, but vanished at larger horizontal gap sizes. This be-

haviour can be explained as follows. The entrained air bends to "crowd" around the L.E. of the quadrant, whereby the velocity and suction pressure on the nozzle underside is reduced, resulting in an increase in L_N.

No connection was found in the variation of L_N with the flow cross sectional area $\propto \sqrt{\ell^2 + a^2}$. This indicates that it is not as much the flow area itself as its position relative to the nozzle which has an effect upon L_N. The pressure distributions were integrated in order to find L_N for a few near optimum configurations. (See also table in next section.)

6.10 Effect of a Rounded L.E. of the Quadrant

In order to investigate the effect of a smoothly curved quadrant L.E. on both L and L_N, a piece of wood was glued to the quadrant as shown in Fig. 24. The quadrant was tilted to the maximum angle $\varepsilon = 12^o$ and the wedge angle of the wood was made 12° so that the piece was vertical. This configuration was then compared with that where the original quadrant is at $\varepsilon = 0^o$ and for the same ℓ and a values. The results for the subsonic nozzle at P.R. = 1.5 and a/t = 6.4, are listed in the table below:

TABLE I

	SHARP L.E.		ROUNDED L.E.	
ℓ/t	3	5	3	5
L (lbs.)	15.63	15.50	18.800	17.030
L_N "	-0.98	-0.98	-4.194	-3.378
L_T	14.65	14.52	14.606	13.652
ϕ	1.31	1.29	1.563	1.418
ϕ_T	1.22	1.21	1.216	1.136
$\Delta\phi = (\phi_T - \phi)$ %	-6.9	-6.2	-22.1	-20.0
D (lbs.)	11.87	11.67	11.99	11.99

This shows that a rounded L.E. does considerably improve entrainment, but what was gained in this way in the form of a larger lift (L) on the test rig was lost by the increase in negative lift L_N. Thus the total thrust augmentation was even slightly smaller in the case of a rounded L.E. of the quadrant. The readings above again indicate that also for the rounded L.E., the optimum ℓ/t ratio is about the same as that for the sharp L.E., i.e., ℓ/t = 3÷4.

The data for L (or ϕ) for the sharp L.E. do not fully agree with readings taken previously for the same configuration, the reason being that the calibration constants of the strain gauge balance had changed slightly during a period of several months which elapsed between both tests. However, this inconsistency does not affect the comparison present in the above table.

6.11 Estimation of Total Thrust Augmentation (ϕ_T)

The values in the table above show that in the case of a sharp L.E. the drop from ϕ to ϕ_T is 3 - 7%. The configuration with $\ell/t = 3$ and $a/t \simeq 6.4$ was found to give a maximum thrust augmentation of $\phi_m = 1.45$ for the untilted quadrant, $\epsilon = 0^o$ (see Fig. 5). The corresponding lift was L = 17.44 lbs. Therefore $L_T = L + L_N = 17.44 - 0.98 = 16.46$ lbs. and $\phi_T = L_T/J_1 = 16.46/12.02 \approx 1.37$, which is 5.5% less than ϕ_m.

When $\epsilon \neq 0^o$, the near optimum configuration was found at $\epsilon = 10^o$ to 12° (Fig. 20). L_N was calculated from pressure distributions for the case of $\epsilon = 12^o$ to be $L_N = -2.7$ lbs. From Fig. 7, the average lift for this configuration was 18.03 lbs. ($\phi = 1.5$); hence $\phi_T = (18.03 - 2.7)/12.02 = 1.273$, which is a drop of 15.1%.

The maximum value of thrust augmentation obtained during all runs with the subsonic nozzle was $\phi_m = 1.545$ at $\epsilon = 10^o$. Assuming a linear increase with ϵ of the lower secondary entrainment, interpolation of $\Delta\phi$ (%) between a value of 5.5% at $\epsilon = 0^o$ and 15.1% at $\epsilon = 12^o$ gives $\Delta\phi = 13.5\%$ at $\epsilon = 10^o$ at which the total thrust augmentation then becomes $\phi_T = 1.545 - 1.545 \times 13.5\% = 1.336$.

Thus by comparing the optimum total thrust augmentation obtained with an untilted ($\phi_T = 1.37$) and a tilted ($\phi_T = 1.336$) quadrant, it seems rather difficult to say which one can be considered as the better configuration.

A series of runs was carried out also with the supersonic nozzle at P.R. = 1.5, 2.0 and 2.77 with the rounded L.E. The lift on the nozzle was calculated from pressure distributions and the ratio L_N/L and $\Delta\phi$ (%) was found to be practically independent of pressure ratio.

For the supersonic nozzle, the drop from ϕ to ϕ_T was about 25% smaller if compared with that for subsonic nozzles (see Table II).

6.12 Flow Velocity Profiles

There were investigated for several near optimum configurations. By means of wool tufts, the general flow picture was found to be as illustrated in Fig. 3, where also the flow cross sectional areas are defined.

The upper and lower secondary flow velocity profiles and the exit flow velocity profile for the subsonic nozzle are shown in Figs. 25 and 26 for the configuration and characteristic values, which follow: P.R. = 1.5, $\epsilon = 12^o$, $\ell/t = 8$, $a/t = 6.4$, $\gamma = 6^o$, $\psi = 2^o$, $\alpha = 40^o$, $\beta = 20^o$, $d/t \simeq 26$, $H/d \approx 6$. Inviscous, incompressible flow theory was employed for the calculations of the velocities.

6.12.1 Upper Secondary Flow Velocity Profile (Figure 25)

The static pressure was measured in the $A2_U$ plane (see Fig. 3) with a rake of longitudinal stations, 1/2" apart. The glass sidewalls enclosed the entire flow cross section, and the velocity was found to be uniform in the lateral direction. The nonuniform velocity profile (in the longitudinal direction, Fig. 25) shows that the flow is speeded up around the lip of the top exterior flap and retarded due to the blockage effect of the settling chamber (near the nozzle lip).

6.12.2 Lower Secondary Flow Velocity Profile

This was calculated from static pressure measurements along the extended midline and the two quarter lines (see Fig. 23). Due to the entrainment from the sides, the velocity had the same nonuniform lateral distributions as found previously over the nozzle itself. The 1/4 line readings (average) are plotted in Fig. 25. $V2_L$ increased strongly toward the L.E. of the quadrant.

6.12.3 Exit Mixing Channel Flow Velocity Profile

The total and static pressures were measured in the exit plane (A_3) along three sections located one inch from each glass plate and along the midline. The calculated velocity distribution is plotted in Fig. 26. It shows that the nonuniform spanwise velocity distribution at the lower secondary flow inlet is still detectable at the outlet. It also shows that the peak velocity occurs close to the exterior flap where the velocity was found to be nearly uniform in the spanwise (lateral) direction. In the plane of symmetry, the exit velocity V_3 at the exterior flap is seen to be about twice the velocity of the interior flap. Wool tufts indicated that in the mid portion of the flow, the velocity had a component toward the exterior flap.

This somewhat unexpected distribution has also been observed in similar experiments performed at DeHavilland Aircraft Co. of Canada Ltd. and at this Institute. Since the velocity peak has shifted toward the exterior flap, one may assume that optimum mixing has been reached. For this particular diffuser, this observation could be caused by the fact that it is not symmetrical with respect to the vertical ($\gamma = 6^o$, $\varphi = 2^o$).

6.13 Estimation of Secondary and Mixed Massflows

For the particular configuration mentioned above, the flow cross section areas were: $A2_U = 49.25$ in^2, $A2_L = 10.0$ in^2, $A_1 = 1$ in^2, A_3 44.8 in^2 and the area ratio $A_2/A_1 = 59.25 \approx 60$. The massflows $\rho \int V dA$ were integrated graphically and found to be: $m_2 = m2_U + m2_L = 0.0558 + 0.0278 = 0.0836$ slugs/sec. The measured primary flow $m_1 = 0.0148$ slugs/sec which "theoretically" adds up to $m_3 = 0.0984$ slugs/sec. Actual measured $m_3 = 0.1030$ slugs/sec. This is a difference of about 4.5%. The mass augmentation is seen to be

$$\mu = \frac{m_3}{m_1} = \frac{0.1030}{0.0148} \approx 7.06$$

If the secondary massflows, obtained with an untilted quadrant ($\varepsilon = 0^o$) but everything else unchanged, is next compared with the above case, it is found that in the latter case m_{2_L} was 17.3% larger, whereas the total secondary massflow m_2 increased by 4.2%. The increase in the thrust augmentation from $\varepsilon = 0^o$ to $\varepsilon = 12^o$ with $\varphi = 2^o$ (see Fig. 8) was about 17% and indicates the connection between ϕ and m_{2_L}. From this it can be concluded that the lift on the Coanda surface was increased by allowing a larger mass flow (or higher velocity V_{2_L}, since $\mathcal{L}$ and a were unchanged) through the lower secondary flow inlet. However, the simultaneous increase in the suction pressure on the bottom surface of the nozzle resulted even in an overall decrease in ϕ_T with the present experimental set-up.

6.14 Mixed Flow Total Momentum (F_3) Compared with L_T

The exit velocity V_3 was squared, plotted and integrated graphically across A_3 to obtain $J_3 = \rho \int V_3^2 \, dA$ for the $\varepsilon = 12^o$ configuration. J_3 was found to be 15.7 lbs. The average exit static pressure $\bar{P}_3$ was $\approx$ 0.6" H_2O below the atmospheric pressure P_a, and $A_3 = 44.8$ in^2. This resulted in a pressure thrust of 0.97 lbs. Thus the total exit momentum becomes

$$F_3 = J_3 + (\bar{P}_3 - P_a) A_3 = 15.7 - 0.97 = 14.73 \text{ lbs.}$$

The measured average total lift L together with the estimated L_N gives then $L_T = 16.03 - 2.70 \approx 15.3$ lbs. This value confirms quite well the theoretical prediction of $F_3 = L_T$, the difference being ≈ 3.7% which most likely is within the accuracy of the measured and integrated exit pressures. Similarly, one gets for $F_1 = J_1 - (P_1 - P_a) A_1 = 12.02 - 0.1 = 11.92$ lbs. The average measured drag D = 11.86 lbs., the estimated $D_N = 1.0$ lbs.; therefore, $D_T = 12.86$ lbs. A comparison of

$$\frac{F_3}{F_1} = \frac{14.73}{11.92} = 1.236$$

and

$$\frac{L_T}{D_T} = \frac{15.3}{12.86} = 1.191$$

indicates about the same percentage difference as above.

6.15 Mixing Efficiency

The mean velocities for this configuration at a P.R. of 1.5 were: $\bar{V}_{2U} = 70.5$ ft/sec, $\bar{V}_{2L} = 173$ ft/sec, $\bar{V}_3 = 143$ ft/sec and $\bar{V}_1 = 825$ ft/sec. Defining the mixing efficiency as the ratio of the kinetic energy of the exit flow to that of the primary, one gets (based on mean velocities)

$$\Omega = \frac{m_3 \bar{V}_3^2}{m_1 \bar{V}_1^2} = 7.06 \times \left(\frac{143}{825}\right)^2 = 7.06 \times 0.1735^2 = 0.212$$

Thus about 79% of the primary kinetic energy is lost during the mixing process due to viscous losses, i.e., turbulence and friction. The values above also illustrate that the massflow ratio m_3/m_1 is increased more than the decrease in the velocity ratio $\bar{V}_3/\bar{V}_1$, with the result of augmentation of the thrust.

6.16 Accuracy

The angles α and β could be set within $\pm 2^o$ accuracy, and ε, γ and φ within $\pm 1^o$. The diffuser inlet width d varied within 0.1" due to the varying suction pressure on the external flaps with different pressure ratios (slack and elastic deformation). Therefore, d/t varies between 26.0 and 26.8. The gap sizes a and ℓ were within $\pm$ 0.03". Due to vibration of the rig during the runs the needle on the strain gauge indicators oscillated somewhat and a mean reading had to be taken. The atmospheric conditions, i.e., wind direction and slipstreams from passing aircraft, were found to affect the inlet air of the engine (and the readings) to a noticeable extent. But in test runs near the optimum configurations, two or more sets of readings were often taken and the scattering of the results (ϕ) was in the worst case 3.4% (taken at different times).

The obtained thrust augmentation ratios ϕ are believed to be accurate well within $\pm$ 5%.

6.17 General Discussion

It has been established that thrust augmentation can be obtained by means of additional surfaces even when the resulting lift force on these surfaces was negative. Furthermore, by increasing the secondary flow entrainment through an additional gap between the nozzle and L.E. of the quadrant, augmentation can be increased because the secondary massflow was increased. This massflow is the more useful the higher its velocity. By increasing the vertical gap (a), a convergent entrance channel is created for the lower secondary massflow, tending to increase V_{2L} (see Fig. 3). This is in principle a similar effect to that created by the upper portions of the exterior flaps whereby V_{2U} is enhanced. In addition, such an additional gap on the jet sheet underside takes advantage of the large entrainment of curved jet sheets at a position, where its velocity is highest.

In this connection it is interesting to note that a thrust augmentation of about 1.06 has been obtained solely by means of a carefully shaped inlet channel to the underside gap between nozzle and Coanda surface (De Havilland Aircraft Co. of Canada Ltd.)

Looking at this observation from a reaction force view point, the increase in the lift (L) obtained by this additional underside entrainment must come from an increase in the lift (L_C) over the Coanda surface itself because L is increased even when L_F is negative. This increase in L_C is the result of a decrease in $\bar{P}_C$ and/or a more favorable pressure gradient along the quadrant surface.

The increase of L with ε is the result of a) a somewhat promoted channel effect b) additional lift acting on the inclined straight surface of the quadrant and c) the tilting of the deflection surface, might possibly tend to turn the exit flow more perfectly vertical. (See also Sec. 6.4.4.)

The optimum horizontal and vertical gap sizes (ℓ/t and a/t) were found to be of about the same order as those obtained by Korbacher (Ref. 3) in his investigations of maximum jet sheet turning efficiences without any thrust augmenting or additional surfaces.

In a self-sustained vehicle which makes use of thrust augmenting devices, all reaction forces created by the induced flow have to be taken into account in order to estimate the total augmentation (ϕ_T). In the present case, the effect of ℓ and a on the nozzle lift (L_N) indicated that a slightly larger ℓ/t and a slightly smaller a/t ratio than those giving maximum ϕ -values, should be chosen in order to achieve maximum total augmentation, (say, $\ell/t \approx 4$ and $a/t \approx 4$). But this again is very dependent upon the shape of the lower secondary air inlet.

The shape and position of the upper secondary intake seems to have a smaller effect on thrust augmentation than the parameters defining the lower intake and the mixing channel (diffuser). (See also Ref. 10.) The obtained figures for ϕ_T in the present experiments are of the same order as those obtained in similar recent tests (Ref. 10).

6.18 Suggestions for the Increase of Thrust Augmentation

The estimation of L_N was here performed in a rather crude way. If the thrust augmentation is to be estimated from the measured forces on the rig, it would be of great importance for the accuracy of the results that also the forces on the nozzle are measured directly and separately or that L_N is included in the total measured force of the rig. An alternative for the determination of ϕ is to exactly measure the total and static pressures across the entire exit area A_3, and by integration obtain an exact value for $F_3 \propto L_T$. For this alternative, no balance would be required.

Based on the findings of the effect which ε has on L and L_N and the favorable effect a rounded quadrant L.E. has on m_{2L}, a configuration as shown in Fig. 24 may be well worth to be tested. Here the deflection surface is extended under the nozzle and forms with it a smoothly convergent entrance channel with a streamline L.E. The resulting suction forces on the nozzle underside are believed to be compensated for by additional lift on the extended deflection surface.

The experiments with a tertiary inlet promised no increase in ϕ. The reason might be, as also stated by Scott (Ref. 10), that it is important to locate the curved inlet close to or at the T.E. of the deflection surface in order to increase ϕ. A tertiary flow inlet arranged as shown in Fig. 24 might therefore increase ϕ, but it is not believed to have as great an effect as a relatively large well shaped inlet at the L.E. Another tertiary gap located slightly below the lip of the top exterior flap where the flow still has some curvature might also possibly contribute to a larger ϕ.

All areas from which the inlet air is drawn should be free of obstructions, and inlets should be streamlined.

7. CONCLUSIONS

These experiments proved the existence of optimum horizontal and vertical gap sizes between the nozzle lip and leading edge of the deflection surface. They were found to be of the order of $\ell/t = a/t = 4$ for both a subsonic and a supersonic jet sheet, and practically independent of the nozzle pressure ratio and the tilt angle (ε) of the quadrant (deflection surface).

The thrust augmentation ratio ϕ (excluding the lift on the nozzle) increased with ε to a possible optimum at $\varepsilon \approx 10^{\circ}$ to 12°. The increase in ϕ due to varying ε from 0° to 10° was about 21%, but there was no obvious gain in the estimated total augmentation ϕ_T (when the lift on the nozzle is included). The highest observed ϕ was at $\varepsilon = 10^{\circ}$, where $\phi = 1.545$, while the highest $\phi_T = 1.37$ was found at $\varepsilon = 0^{\circ}$. At $\varepsilon = 10^{\circ}$, $\phi_T \approx 1.34$.

Thrust augmentation was smaller with a supersonic jet sheet than with a subsonic one, and both ϕ and ϕ_T decreased with increasing pressure ratios.

Experiments with an additional tertiary entrainment slightly below the T.E. of the deflection surface suggest no increase in ϕ.

The use of a rounded L.E. on the quadrant led to an increase in the entrained massflow and ϕ, but not in ϕ_T with the present rig.

The best diffuser configuration seemed to be for a length to width ratio of about 6 and a total enclosed angle of 8°. The lift force on the exterior flap was in general negative (except near the optimum configuration), but even then there was thrust augmentation.

Best observed ϕ_T in Part I: 1.21

Best observed ϕ_T in Part II: 1.37

REFERENCES

1. Bailey, A.B. — Study of the Coanda Effect, Part I, Use of Coanda Effect for the Deflection of Jet She Over Smoothly Curved Surfaces. UTIA Te Note No. 49, Aug. 1961.

2. Roderick, W.E.B. — Study of the Coanda Effect, Part II: Use o the Coanda Effect for the Deflection of Jet Over Smoothly Curved Surfaces. UTIA T Note No. 51, Sept. 1961.

3. Korbacher, G.K. — The Coanda Effect at Deflection Surfaces Detached from the Jet Nozzle, Can. Aero. and Space Journal, Vol. 8, No. 1, Jan.

4. Hope-Gill, C.D. — An Experimental Investigation into the Sh of Thrust Augmenting Surfaces in Conjun with Coanda-Deflected Jet Sheets (Part I), UTIAS Tech. Note No. 70, May, 1964.

5. Palouste 500 Series, Technical Data, Iss November, 1957, Publication No. 10 Blackburn-Turbomeca.

6. Instructions for Bailey Meters. G22-1, 1959, Form A1201-1159.

7. Chisholm, R.G.A. — Design and Calibration of an Air Ejector t Operate Against Various Back Pressures, UTIA Tech. Note No. 39, Sept. 1960.

8. Von Karman, T. — Theoretical Remarks on Thrust Augmenta Reissner Anniversary Volume - Contribu to Applied Mechanics, 1949.

9. Drummond, A.M., Gould, D.G. — Experimental Thrust Augmentation of a Variable Geometry, Two-Dimensional, Central Nozzle Ejector. Can. Aero. and Space Journal, Oct. 1962.

10 Scott W.J. — Experimental Thrust Augmentation of a Variable Geometry, Two-Dimensional Co Wall Jet Ejector. National Research Cou of Canada, Aeronautical Report LR-394,

APPENDIX A

Primary Massflow Calculation

The expression for the primary massflow m is given in Ref. 6 as

$$m = \frac{E \times 21.4 \times D^2 \sqrt{h_w \times P}}{\sqrt{G \times T}} \qquad \left(\frac{\text{cu. ft.}}{\text{hr}} \text{ at 30'' Hg abs. and } 60^{\circ}\text{F}\right)$$

where
- E = capacity factor
- G = specific gravity of manometer fluid
- T = flowing temperature ($^{\circ}R$)
- P = flowing pressure (psi a)
- D = internal pipe diameter (inches)
- h_w = maximum differential head of fluid meter ("H_2O at $68^{\circ}F$)

Inserting the actual values, this reduces to

$$m = 18.93 \sqrt{\frac{h_w \times P_o}{T}} \quad \left(\frac{\text{cu. ft.}}{\text{sec.}}\right)$$

In order to reduce the amount of work involved in the data reduction, a representative average atmospheric pressure based on all runs was chosen: P_a = 29.3 "Hg = 14.33 psi.

Assuming a deviation from this value of ± 1" Hg (which was about the maximum that was ever observed), the corresponding change in the massflow was less than 3%.

The measured primary flow temperature during all runs was very close to 60°F. Since the pipe flow is low (e.g., at P.R. = 1.5, $V_{pipe} \simeq$ 12 ft/sec), the measured temperature was taken as the primary total temperature T_o. Then

$$\rho_a \simeq \frac{29.3}{30.0} \times 0.002378 = 0.00232 \text{ slugs/cu. ft.}$$

and

$$m = 18.93 \times 0.002378 \sqrt{\frac{h_w \times P_o}{T_o}} \quad \left(\frac{\text{slugs}}{\text{sec}}\right)$$

or

$$m\sqrt{T_o} = 0.044 \sqrt{h_w \times P_o} \quad \left(\frac{\text{slugs} \sqrt{^{\circ}R}}{\text{sec}}\right) \qquad (1)$$

where P_o is given by the relevant pressure ratio P_o/P_a.

The observed mean values of h_w were 2.65"H_2O at P.R. = 1.5 for both nozzles, and for the supersonic nozzle h_w = 3.90"H_2O and 5.75"H_2O at P.R. = 2.0 and 2.77 respectively. The massflows are listed in the next table.

Calculation of Primary Exit Velocity Assuming Isentropic Flow

The following assumptions are made at the exit of the nozzle:

$$P_1 = P_a \text{ and } T_1 = T_a$$

$$V_1 = a_1 M_1 = \sqrt{k R T_1} \cdot M_1 = k R \sqrt{\frac{T_a}{T_o}} \cdot \sqrt{T_o} \cdot M_1$$

$$M_1 = \sqrt{\frac{2}{k-1}\left[\left(\frac{P_o}{P_a}\right)^{\frac{k-1}{k}} - 1\right]}$$

$$\frac{T_a}{T_o} = \left(\frac{P_o}{P_a}\right)^{-\frac{k-1}{k}}$$

Therefore

$$\frac{V_1}{\sqrt{T_o}} = \sqrt{\frac{2 k R}{k-1}\left[\frac{(P_o/P_a)^{\frac{k-1}{k}} - 1}{(P_o/P_a)^{(k-1)/k}}\right]}$$

With k = 1.4 and R = 1716 $ft^2/sec^2\ {}^oR$

$$\frac{V_1}{\sqrt{T_o}} = \sqrt{1200 \times \frac{(P_o/P_a)^{0.286} - 1}{(P_o/P_a)^{0.286}}} \quad \left(\frac{ft}{sec\ \sqrt{{}^oR}}\right)$$

The values of $V_1/\sqrt{T_o}$ are given in the next table.

Primary Momentum Flux (J_1)

J_1 is calculated from Eqs. (1) and (2) and listed in the Table below:

	P.R. =	$m_1\sqrt{T_o}$	$V_1/\sqrt{T_o}$	$m_1\sqrt{T_o} \times \frac{V_1}{\sqrt{T_o}} = J_1$
	$\frac{P_o}{P_a}$	$\frac{slugs \times \sqrt{^oR}}{sec}$	$\frac{ft}{sec\sqrt{^oR}}$	lbs.
Subsonic and Supersonic Nozzle	1.5	0.332	36.2	12.02
Supersonic Nozzle	2.0	0.465	46.5	21.6
	2.77	0.665	55.25	36.75

Primary Nozzle Thrust and Performance

The total thrust of the nozzle is

$$TH_T = J_1 + (P_1 - P_a)\,A_1 = F_1 \qquad (3)$$

If $P_1 \neq P_a$, then J_1 will vary according to Eq. (2) if the actual P_1 is applied instead of P_a. Thus, if $P_1 < P_a$ as was the case in these experiments, the pressure term gives a negative contribution to the thrust while J_1 becomes somewhat larger.

For example at P.R. = 2.77, the total thrust as calculated by Eq. (3), with P_1 instead of P_a in Eq. (2), was found to be practially the same as the thrust calculated by $TH = J_1 = m_1 V_1$ based on P.R. = P_o/P_a. Therefore, it seems justified to neglect any pressure thrust, i.e., to use $P_1 = P_a$ in the calculations.

Next, the ideal isentropic massflow m_1 is compared with the measured m_1. The ideal isentropic massflow is given by

Subsonic Nozzle: $$m_1\sqrt{T_o} = \rho_1 A_1 \frac{V_1}{\sqrt{T_o}} T_o$$

Supersonic Nozzle: $$m_1\sqrt{T_o} = \rho^* V^* A^* \sqrt{T_o} = \rho^* a^* A^* \sqrt{T_o}$$

$$= \left(\frac{2}{k+1}\right)^{\frac{k+1}{2(k-1)}} \rho_o\, a_o A^* \sqrt{T_o} = 0.579\, \rho_o\, a_o A^* \sqrt{T_o} \; (k = 1.4)$$

Here the nominal $A_1 = A^* = 1\ in^2$, $k = 1.4$, the speed of sound is

$$a_o = 49 \sqrt{T_o} \text{ ft/sec, and } T_o = 520^o R.$$

Example: For P.R. = 2.0, $\rho_o = 2 \times 0.00232 = 0.00464$ slugs/ft^3

and

$$\frac{V_1}{\sqrt{T_o}} = 46.5 \text{ ft/sec} \sqrt{^o R}$$

$$m \sqrt{T_o} = 0.579 \times 0.00464 \times 49 \times 520 \ \frac{1}{144} = 0.476 \ (\text{slugs} \sqrt{^o R}/\text{sec})$$

which means that the measured $m_1 \sqrt{T_o} = 0.465$ is $\simeq$ 2.3% (-2.3%) smaller than the ideal isentropic ($m_1 \sqrt{T_o}$).

The corresponding values for P.R. = 1.5 and 2.77 are -2.92% and 0.76% respectively. The variations in the ideal and the measured primary massflows are due to one or more of the following reasons:

1) the flow is not purely isentropic,

2) the throat areas are not exactly equal to the nominal values.

The difference between the momentum flux as calculated by ($m_{ideal} \times V_{ideal}$) and ($m_{measured} \times V_{ideal}$) is naturally of the same order as the difference between the two massflows. Since this varies with type of nozzle and pressure ratio it, seems most practical to express the thrust of the nozzle as

$$TH = J_1 = m_{1_{measured}} \times V_{1_{ideal}} .$$

The values for J_1 shown in the previous table are calculated in this way.

TABLE II

Configuration: Tilt of Quadrant, $\varepsilon = 12^{o}$
Rounded L. E.
a/t = 6.4
Supersonic Nozzle

	P.R. = 1.5		P.R. = 2.0		P.R. = 2.77	
ℓ/t	3	5	3	5	3	5
L (lbs.)	17.870	17.280	31.750	30.40	50.300	46.600
L_N "	-2.612	-2.235	-4.618	-3.91	-7.394	-6.065
L_T "	15.258	15.045	27.132	26.49	42.906	40.535
ϕ	1.487	1.438	1.470	1.468	1.369	1.268
ϕ_T	1.270	1.252	1.257	1.228	1.170	1.104
$\Delta\phi = (\phi_T - \phi)$ %	-15.3	-14.0	-14.5	-12.8	-14.5	-13.0
D (lbs.)	11.33	11.95	20.75	21.16	35.21	36.2



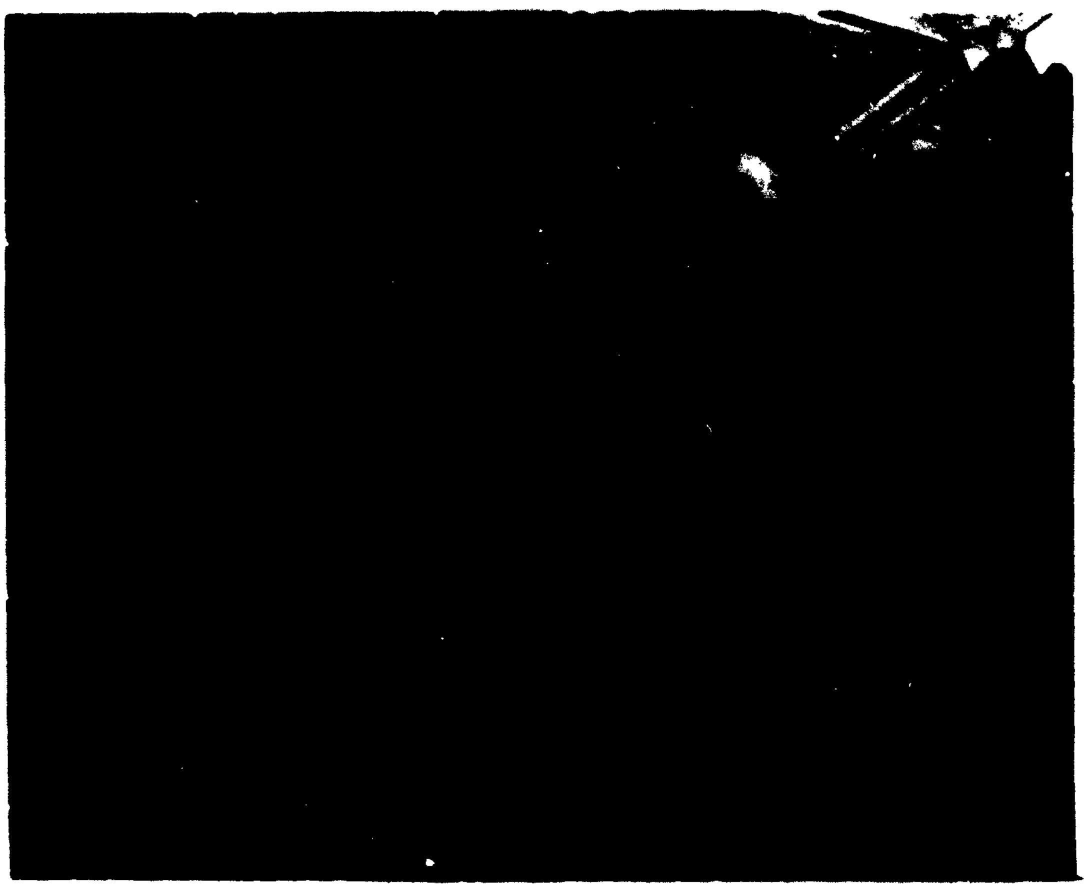


FIG 1 THE THRUST AUGMENTING SURFACES, QUADRANTS AND NOZZLE

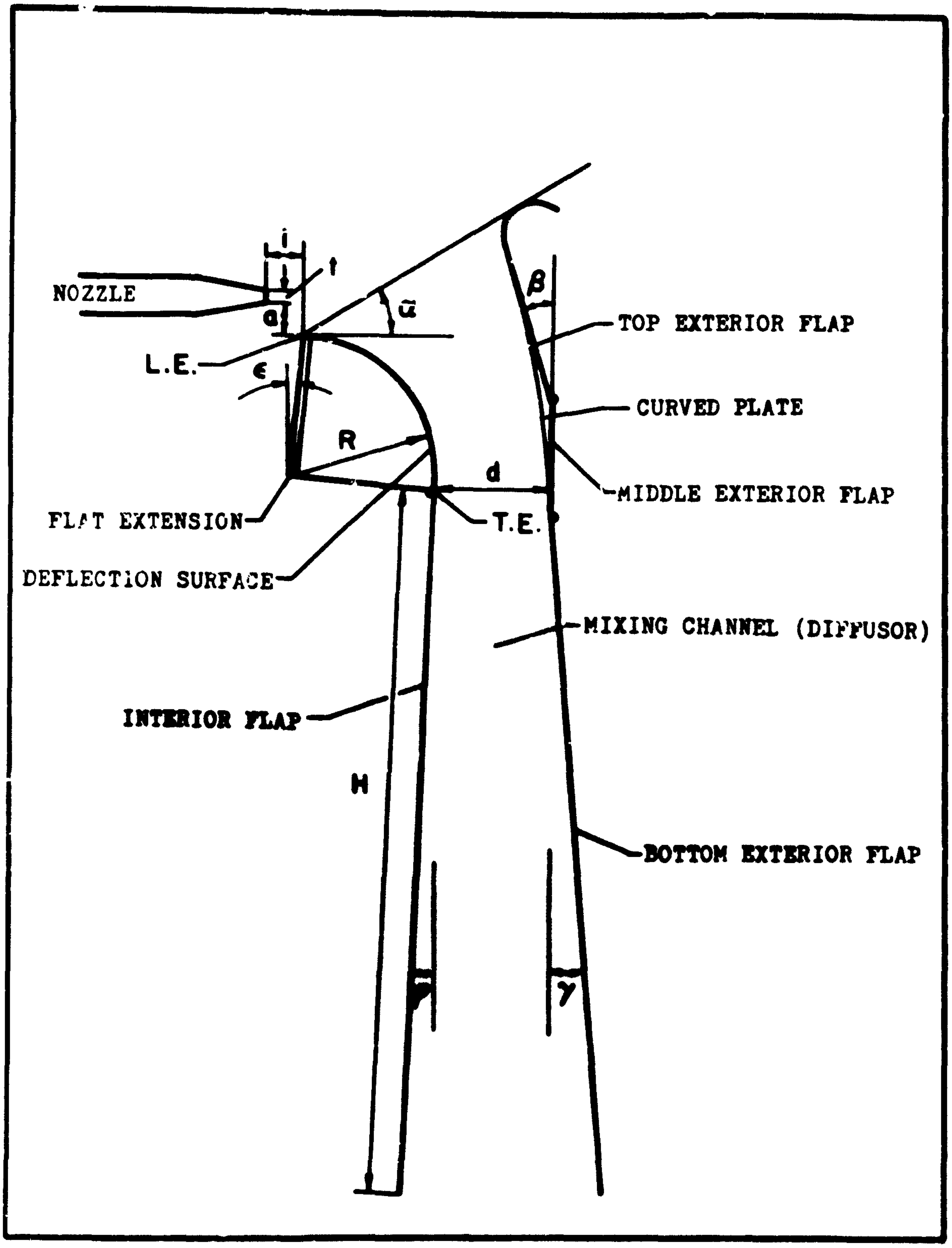


FIG. 2 SYMBOLS AND DEFINITIONS

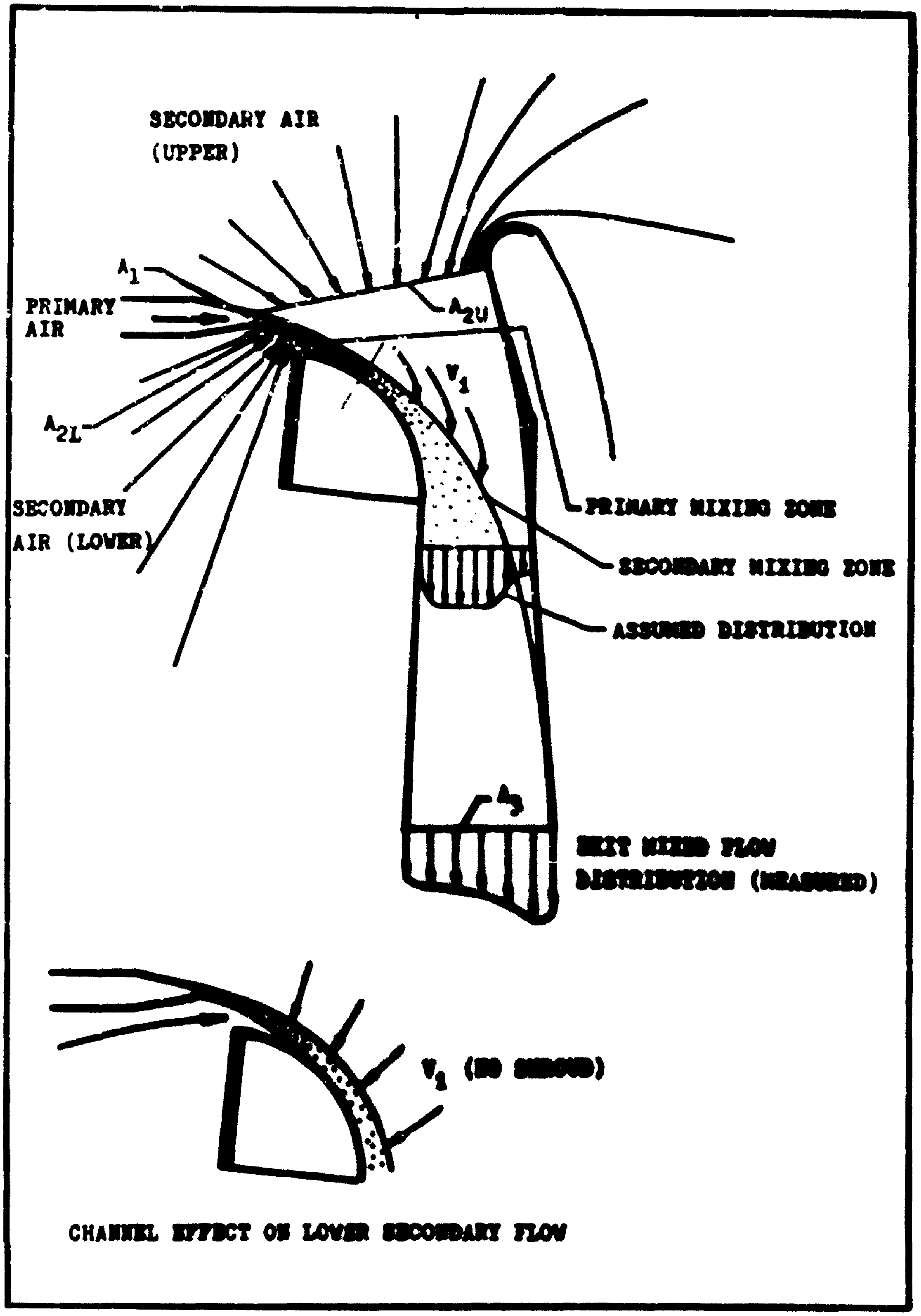


FIG. 3 GENERAL FLOW PICTURE - NOTATION

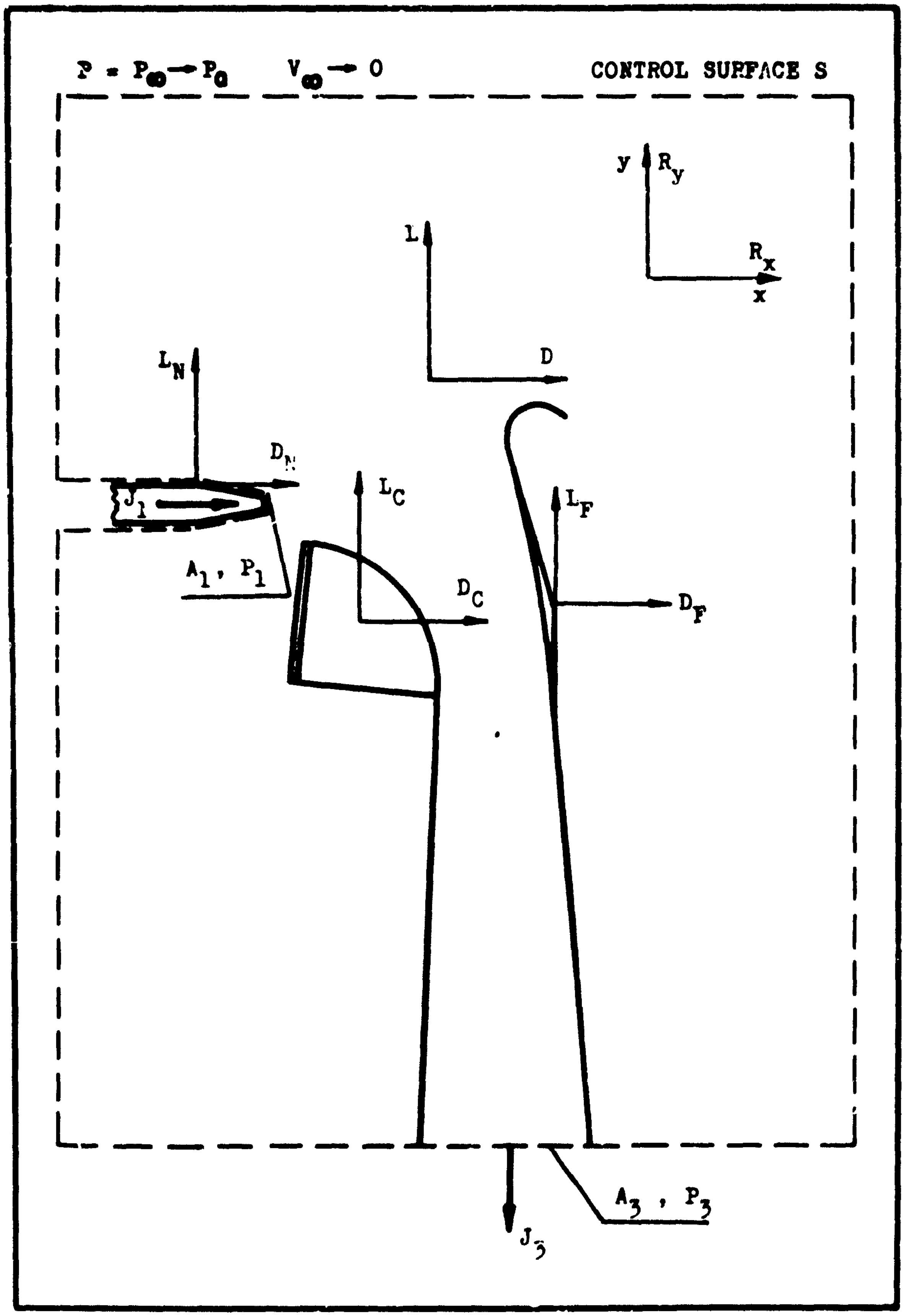


FIG. 4 A PARTICULAR THRUST AUGMENTING SYSTEM (TWO-DIMENSIONAL)

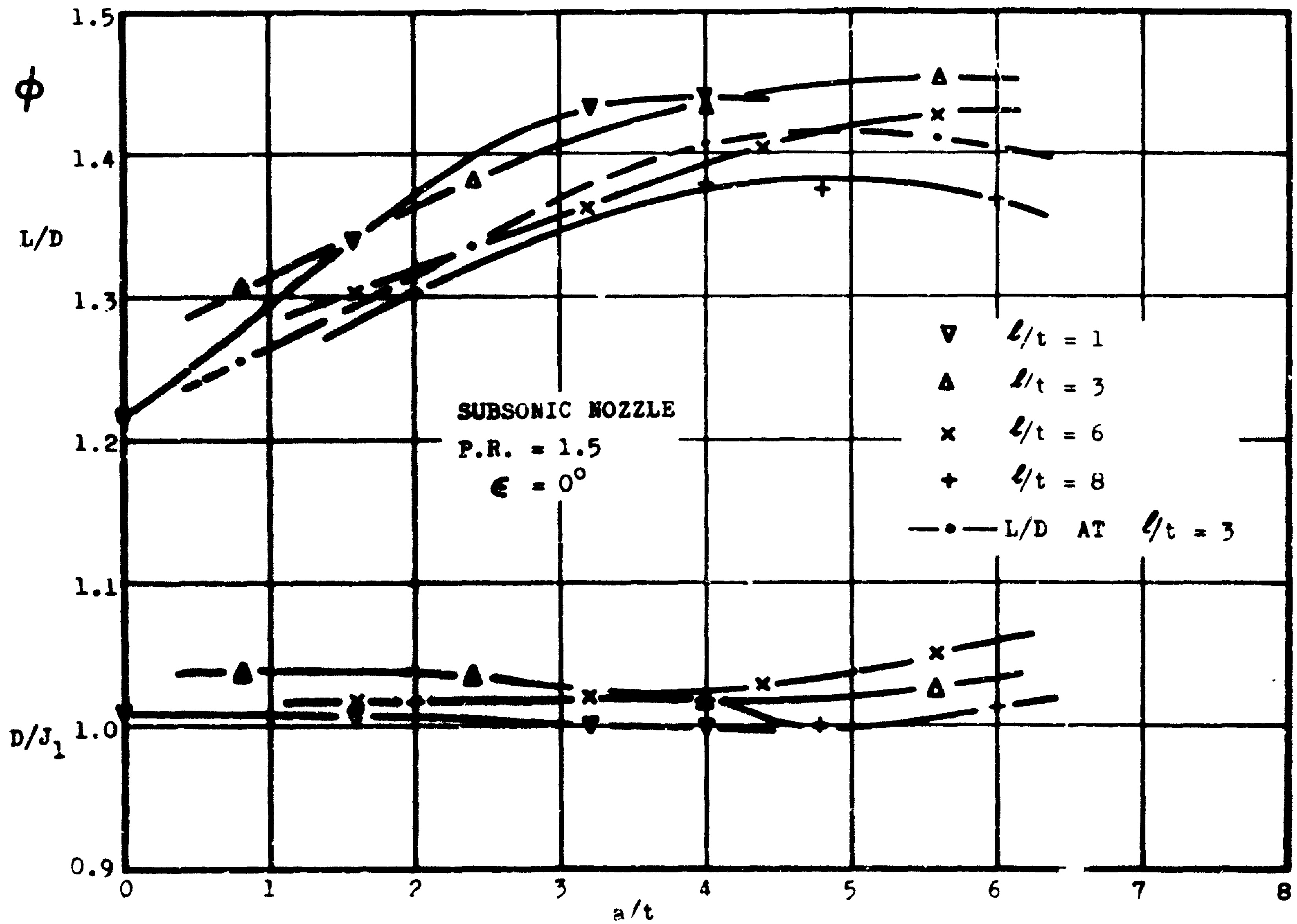


FIG. 5 PLOT OF ϕ, D/J_1 AND L/D VS. a/t FOR VARIOUS ℓ/t RATIOS

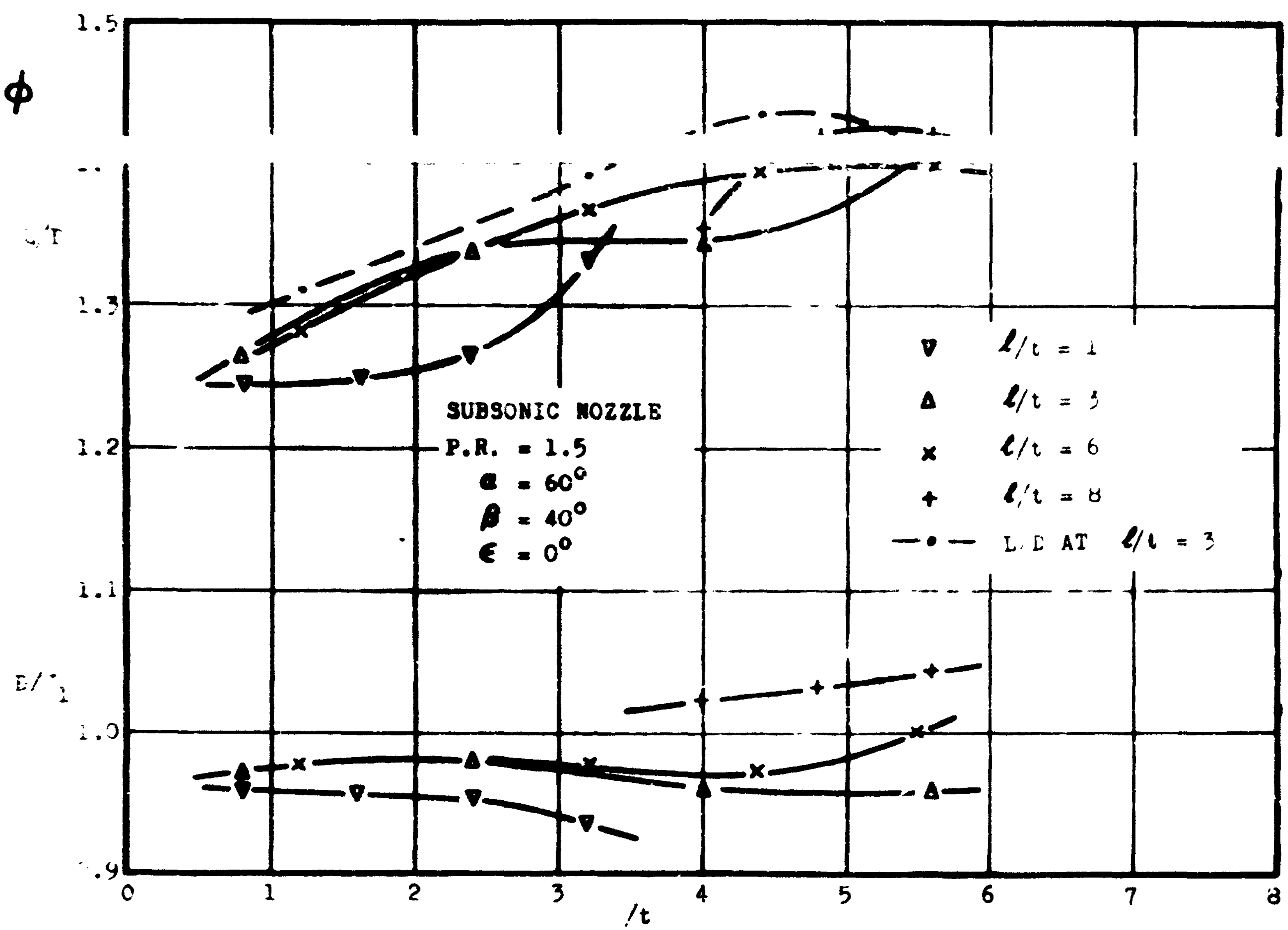


FIG. 6 PLOT OF ϕ, D/J_1 AND L/D VS. a/t FOR VARIOUS ℓ/t RATIOS

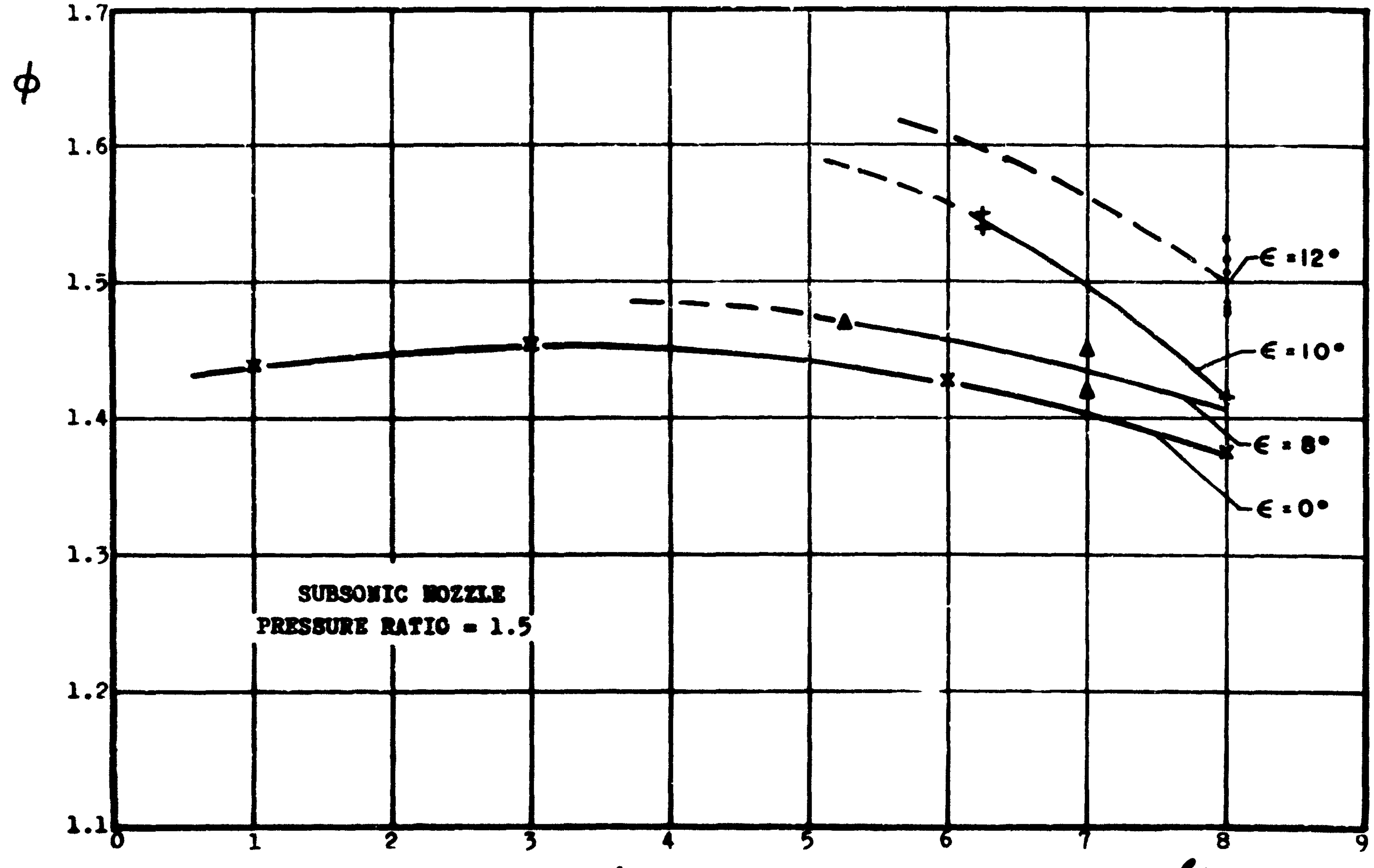


FIG. 7 VARIATION OF ϕ_m VS. ℓ/t FOR VARIOUS VALUES OF ϵ

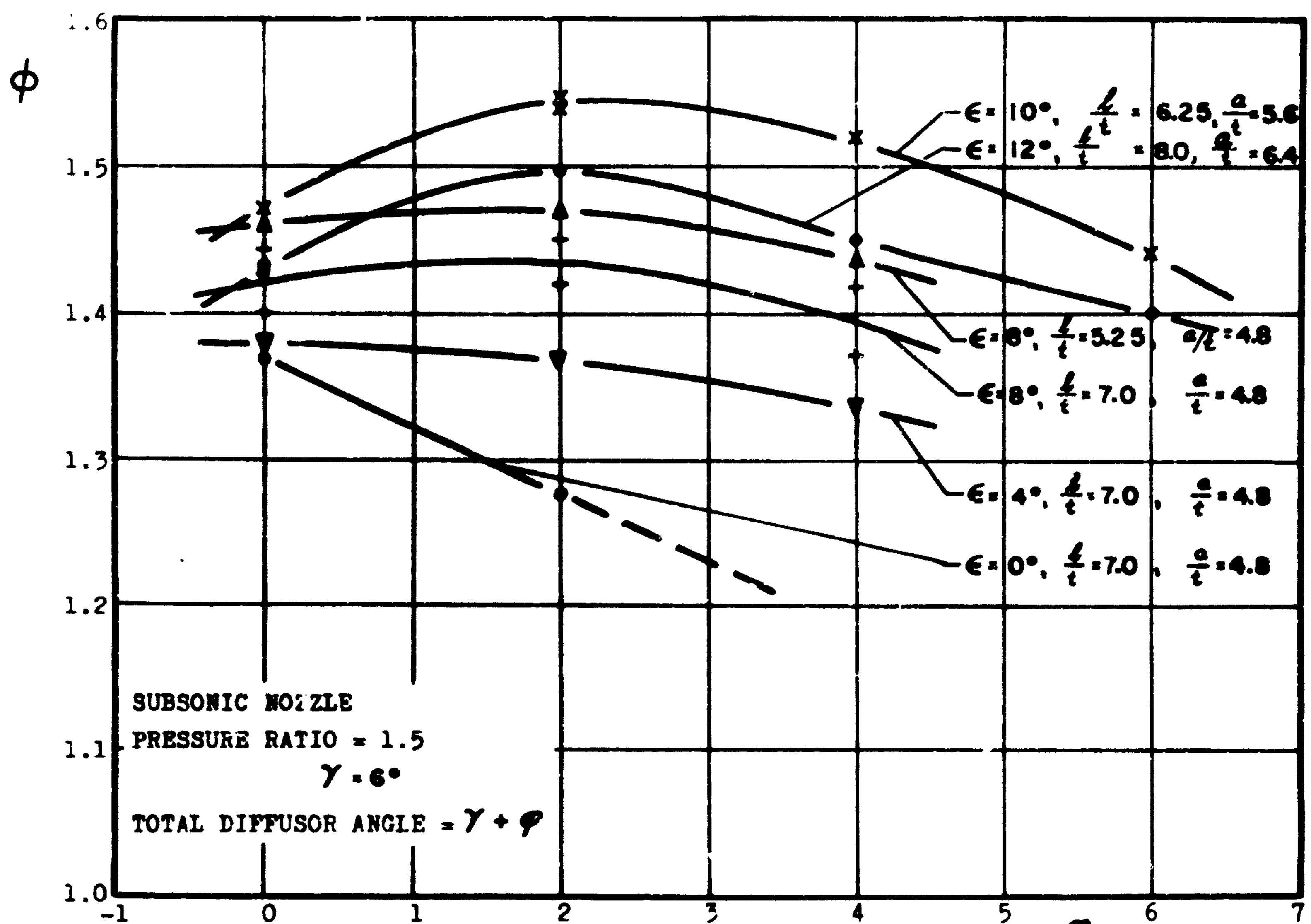


FIG. 8 VARIATION OF ϕ WITH INTERIOR FLAP ANGLE φ FOR VARIOUS VALUES OF ϵ

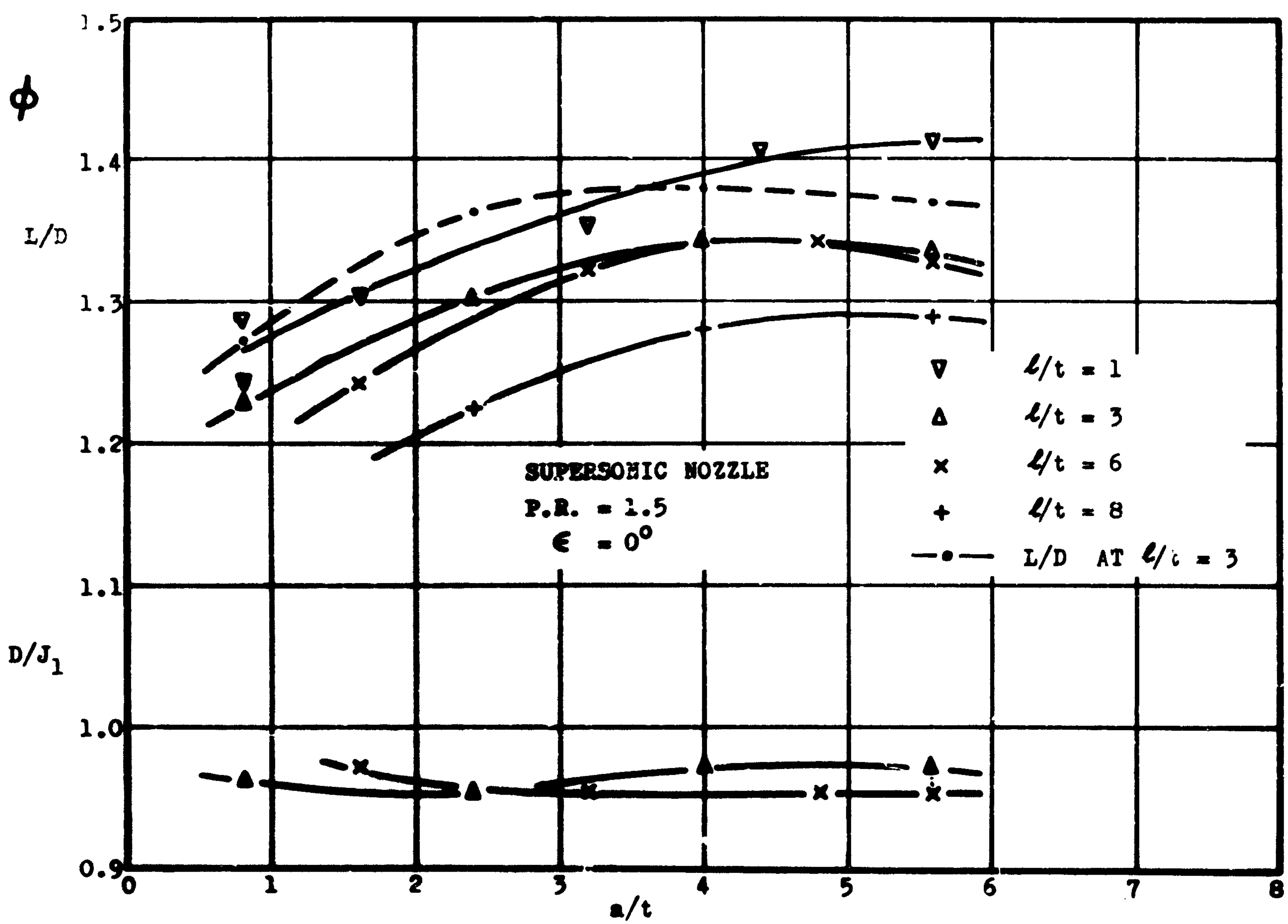


FIG. 9 PLOT OF ϕ , D/J_1 [illegible] VS. a/t FOR VARIOUS ℓ/t RATIOS

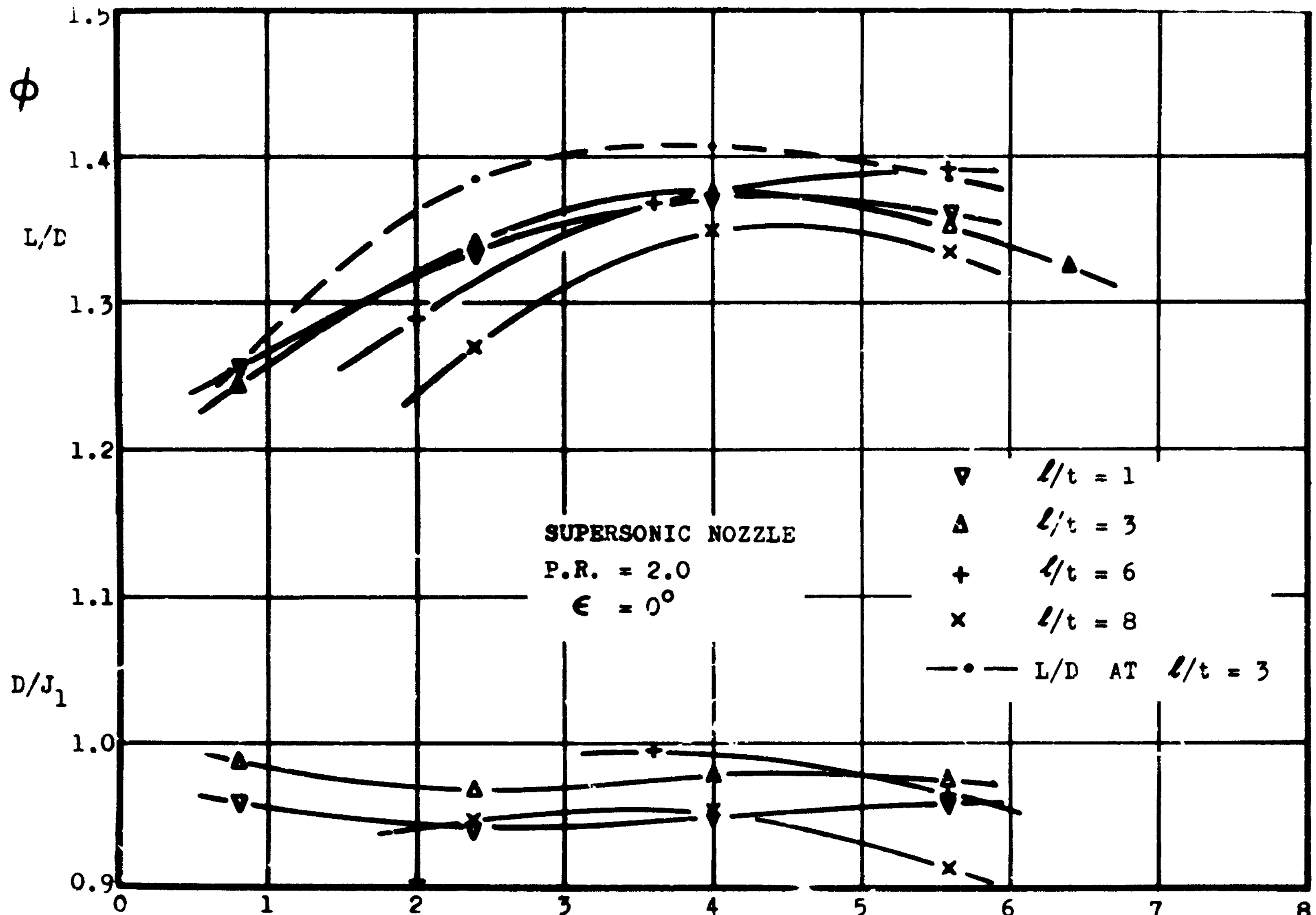


FIG. 10 PLOT OF ϕ , D/J_1 AND L/D VS. a/t FOR VARIOUS ℓ/t RATIOS

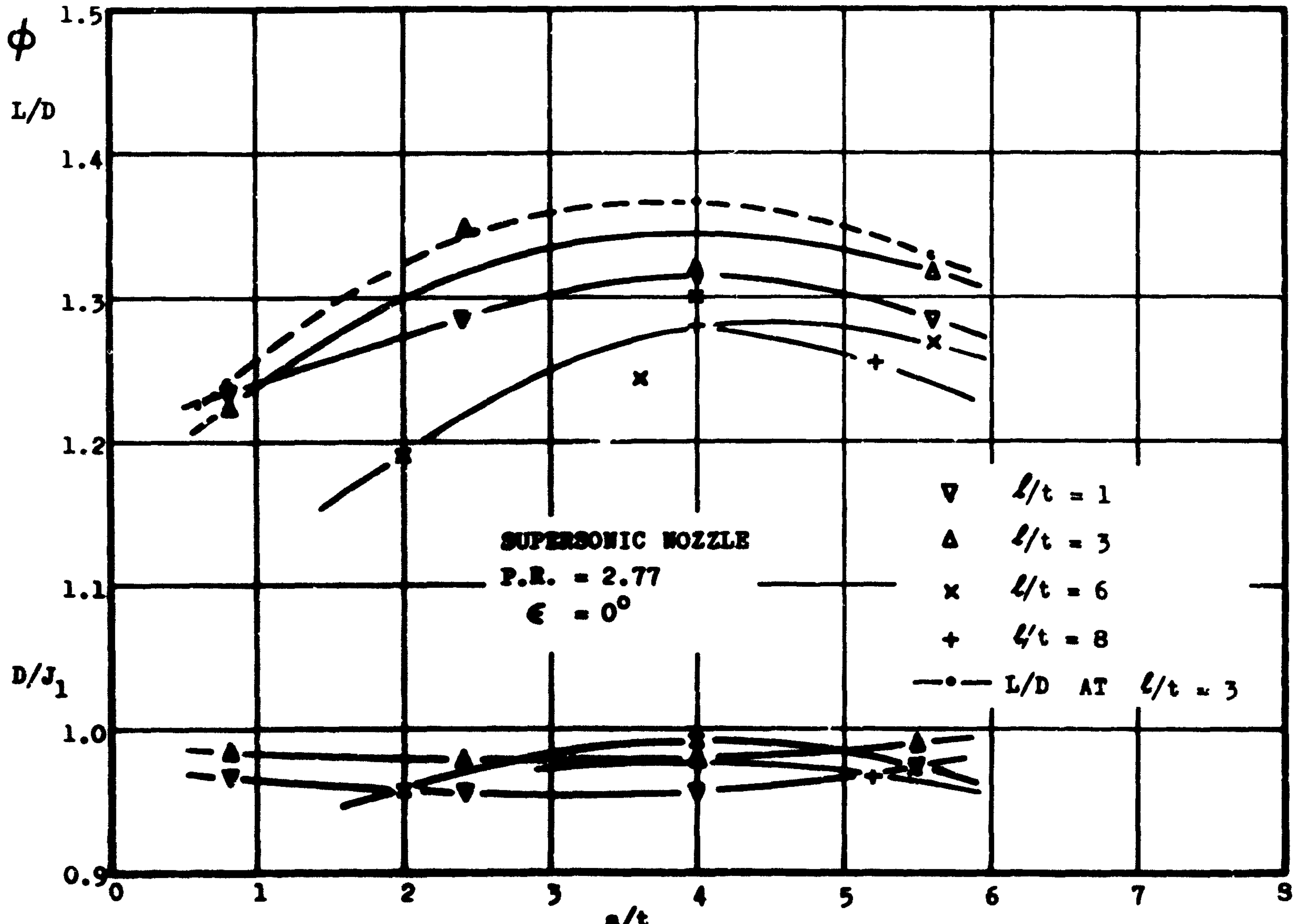


FIG. 11 PLOT OF ϕ , D/J_1 AND L/D VS. a/t FOR VARIOUS ℓ/t RATIOS

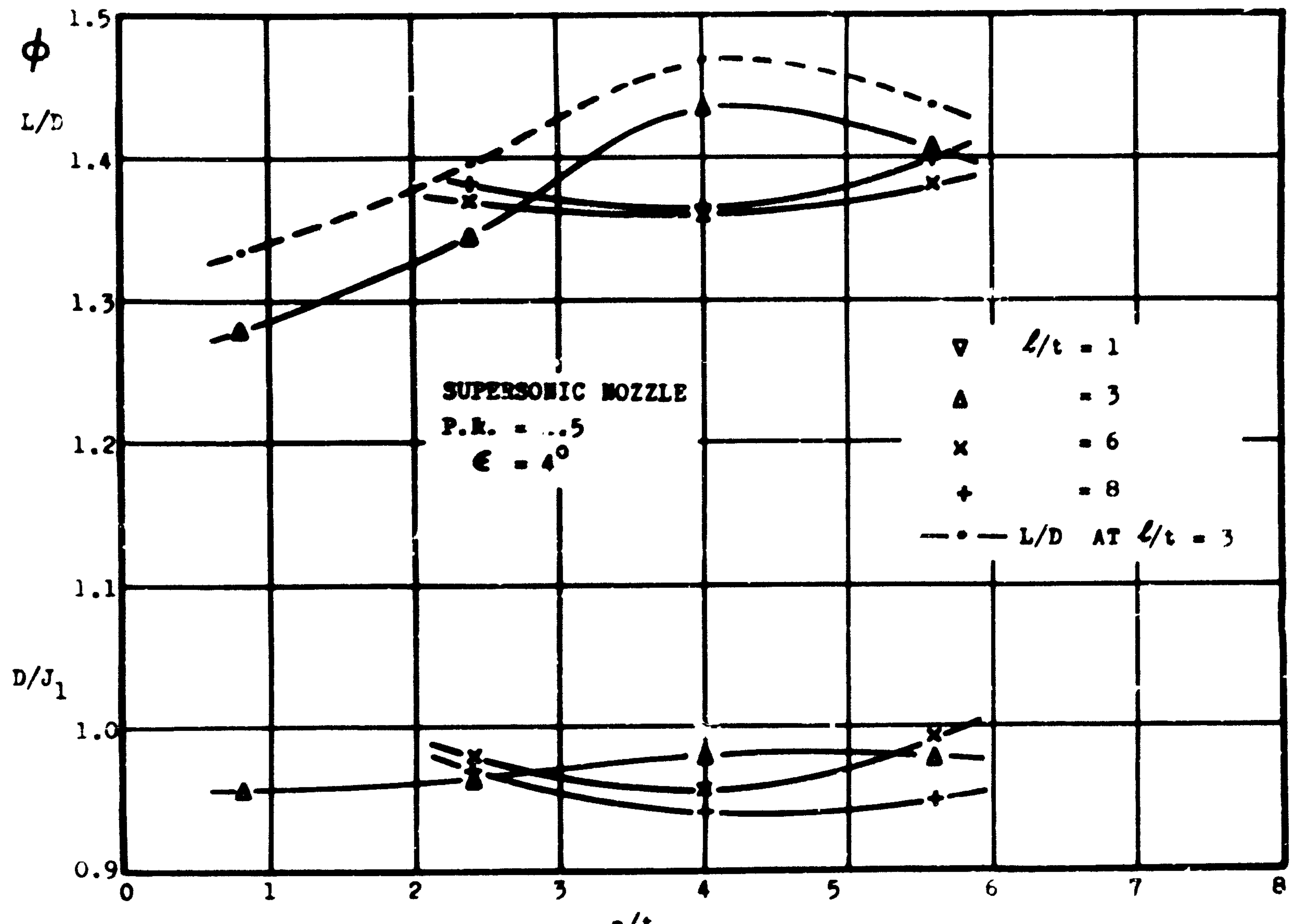


FIG. 12 PLOT OF ϕ, D/J_1 AND L/D VS. a/t FOR VARIOUS ℓ/t RATIOS

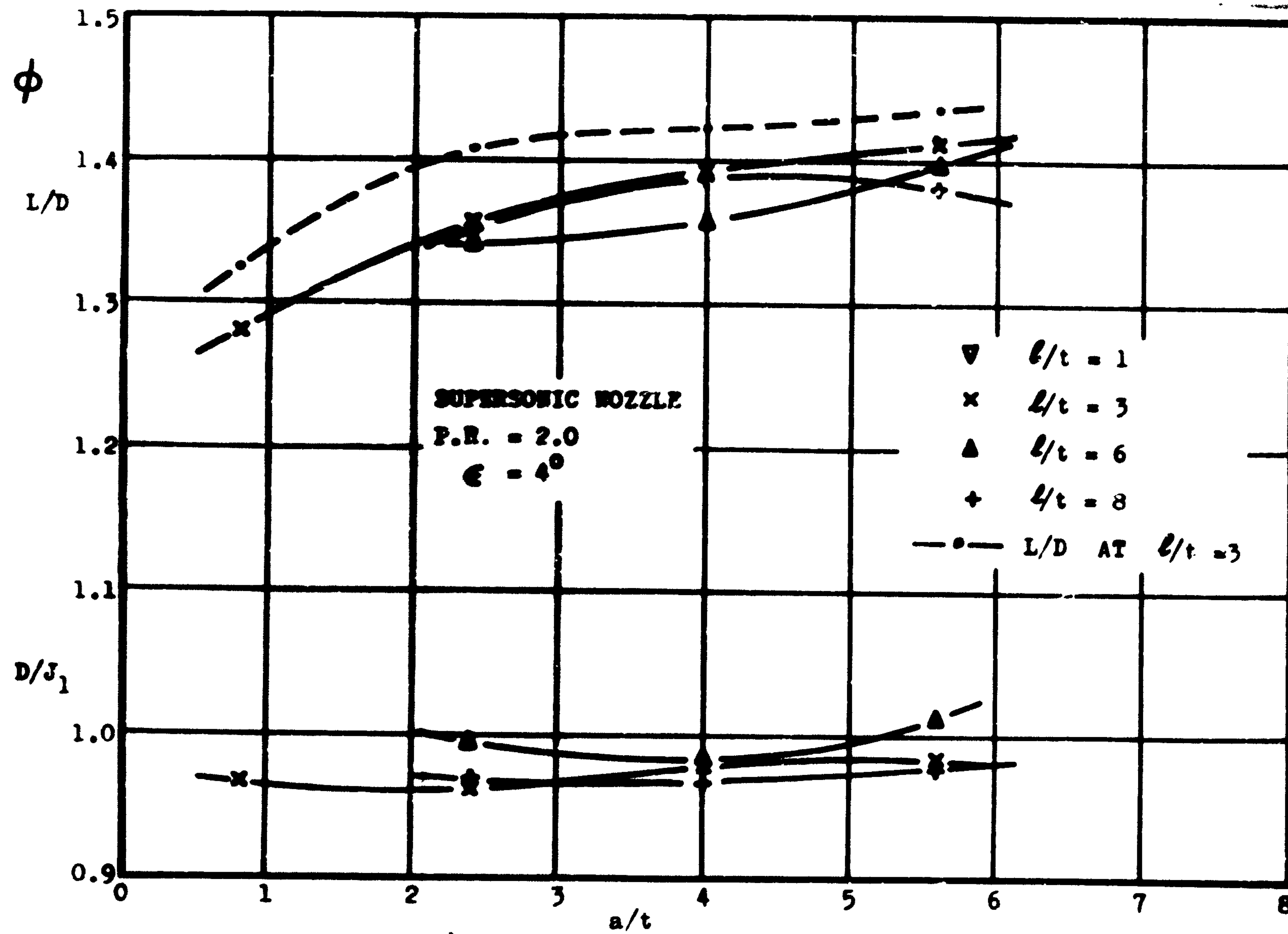


FIG. 13 PLOT OF ϕ, D/J_1 AND L/D VS. a/t FOR VARIOUS ℓ/t RATIOS

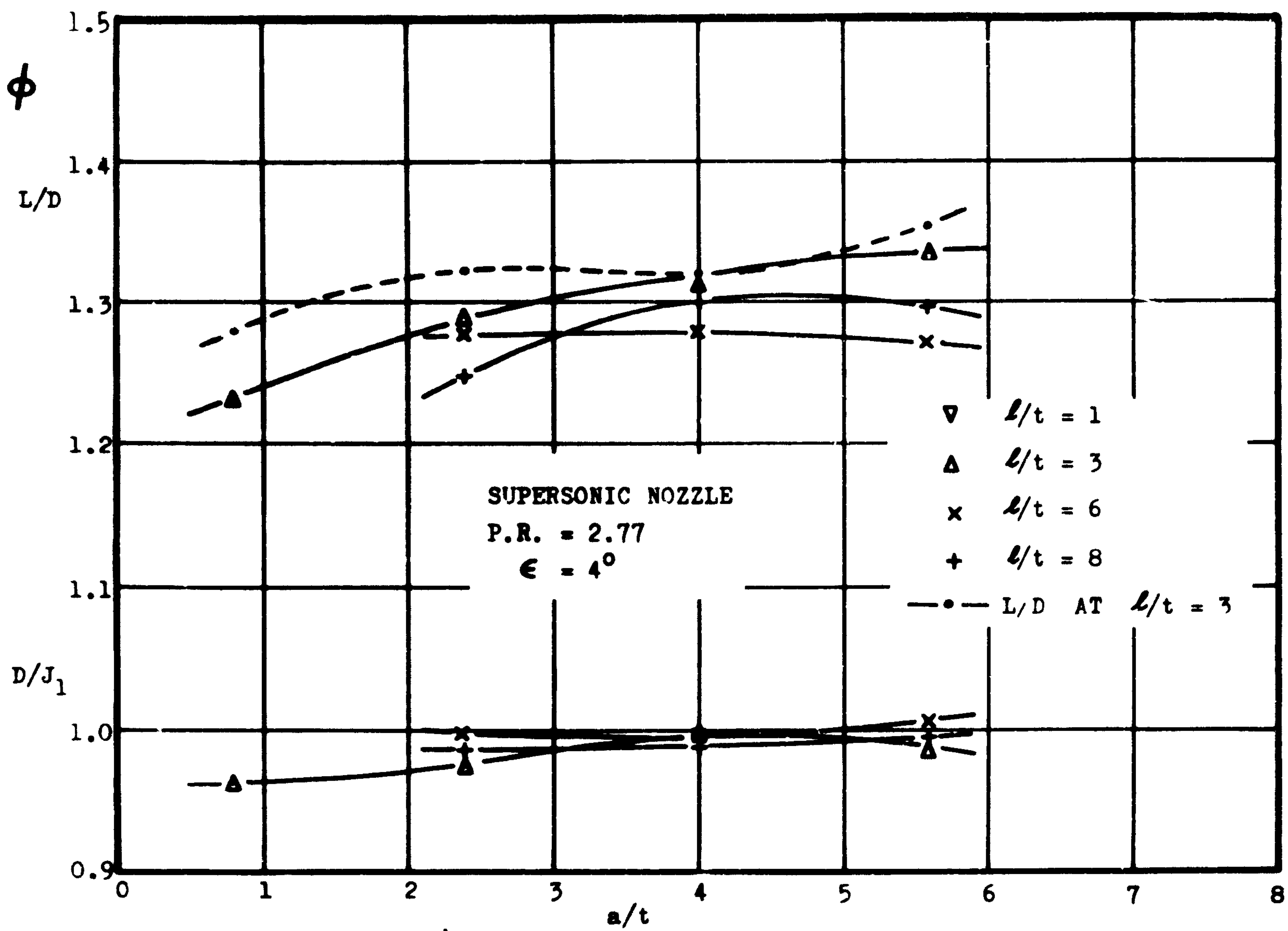


FIG. 14 PLOT OF ϕ , D/J_1 AND L/D VS. a/t FOR VARIOUS ℓ/t RATIOS

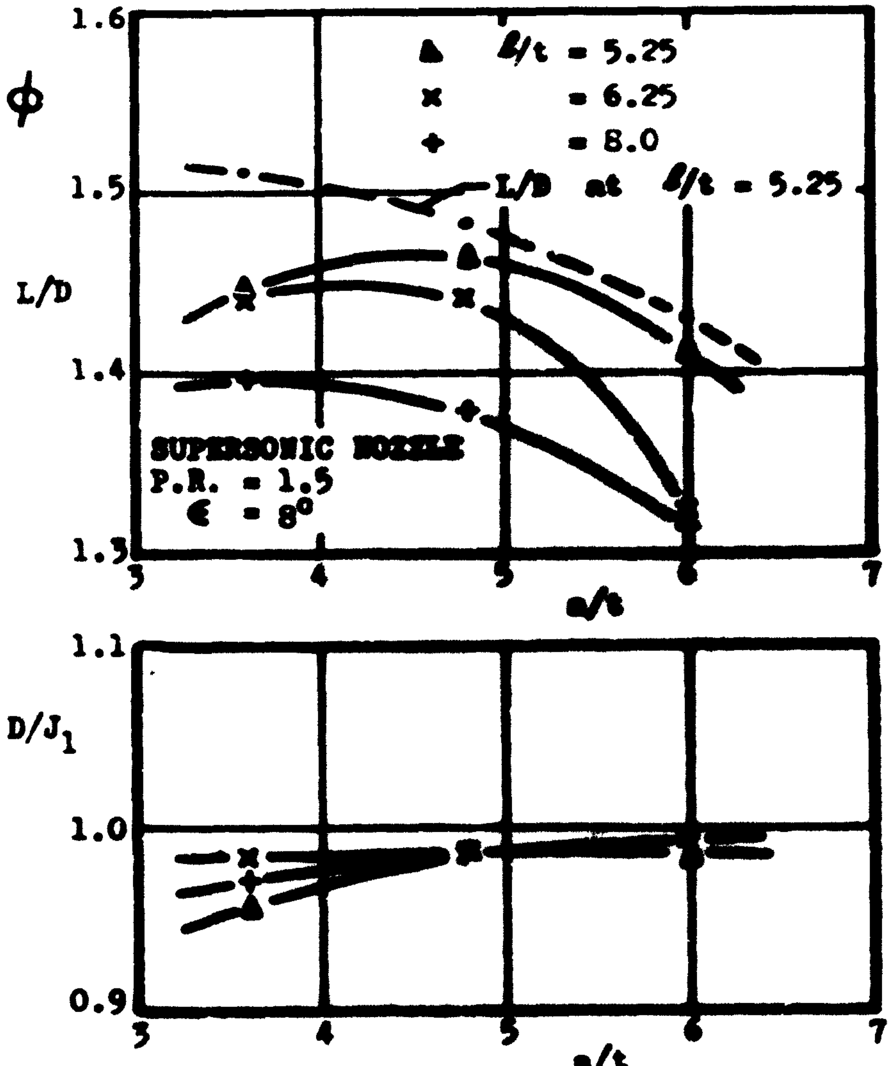


FIG. 15

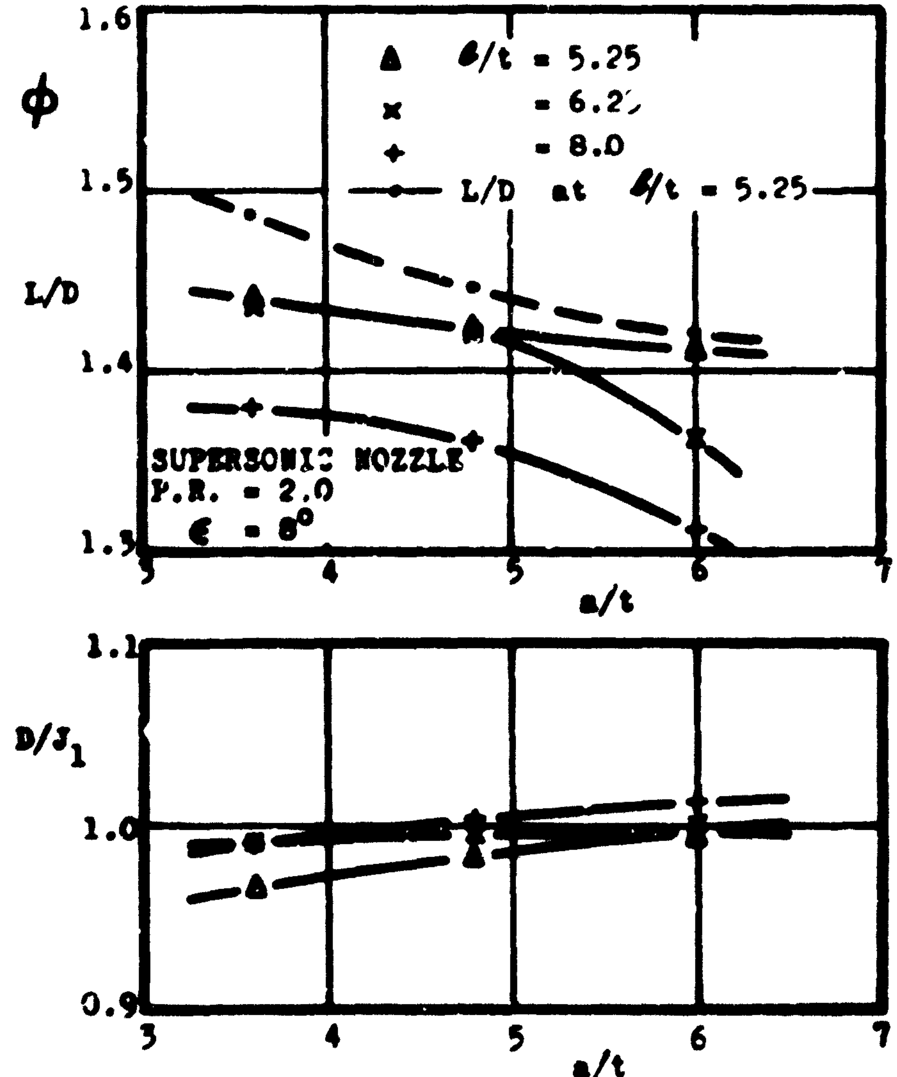


FIG. 16

PLOT OF ϕ, I/J_1 AND L/D VS. a/t FOR VARIOUS ℓ/t RATIOS

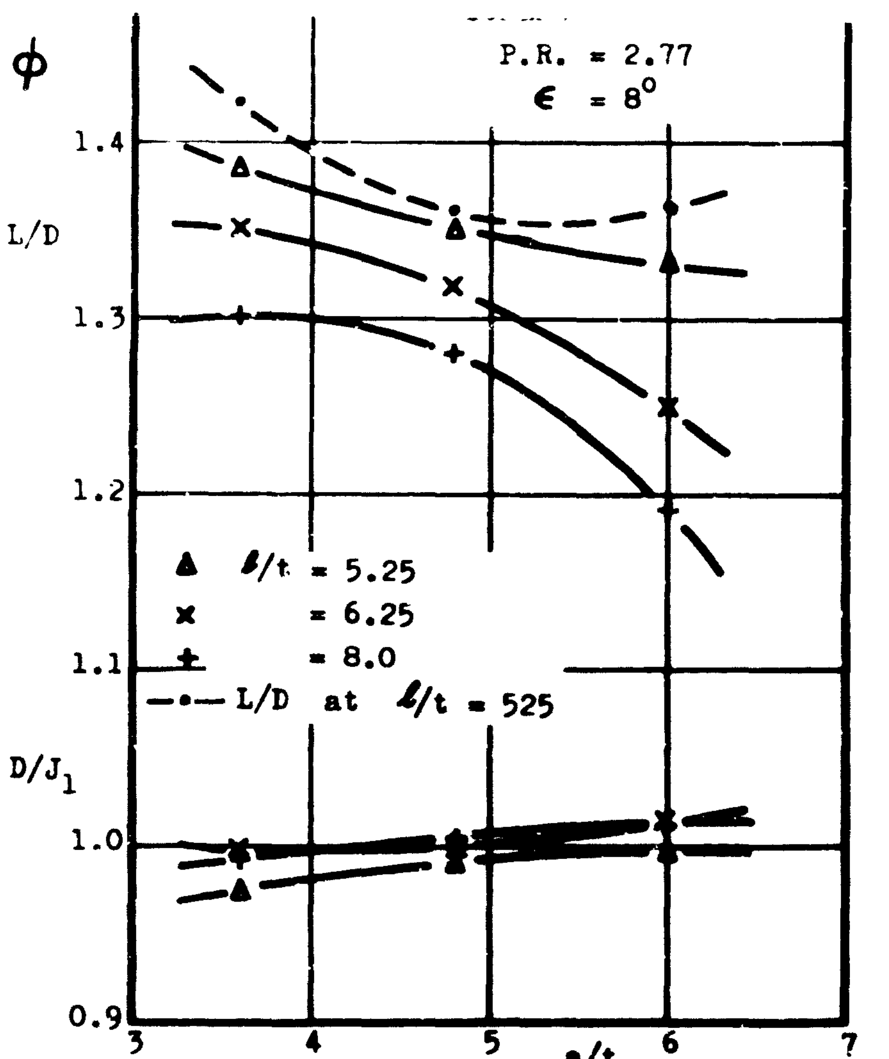


FIG. 17 PLOT OF ϕ , D/J_1 AND L/D VS. a/t FOR VARIOUS ℓ/t RATIOS

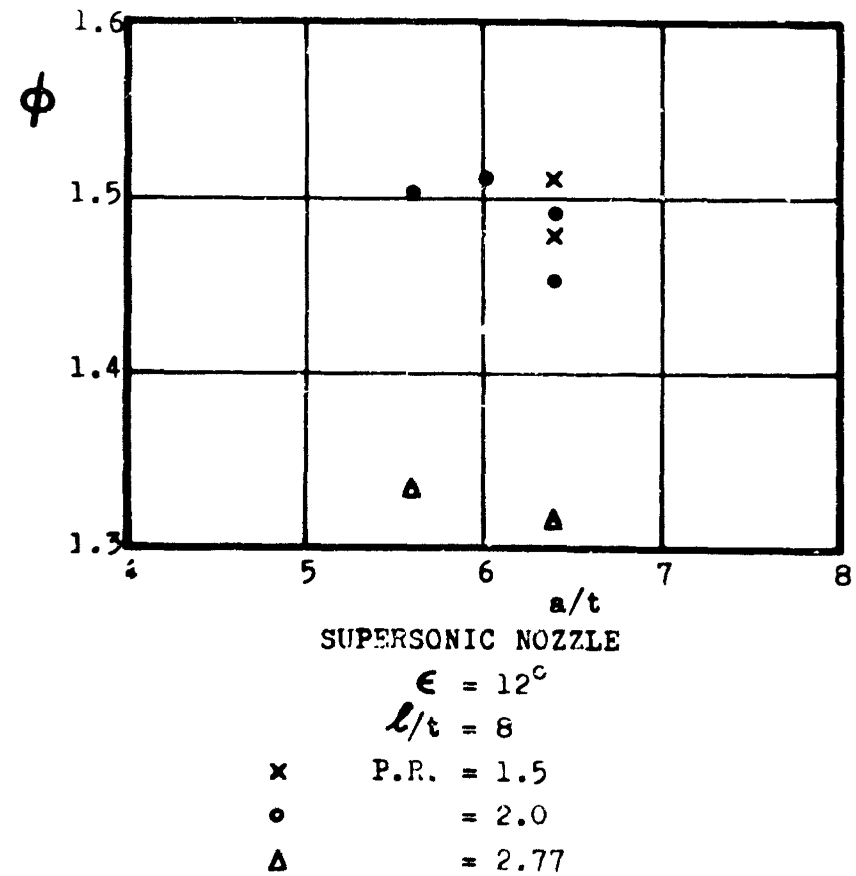


FIG. 18 PLOT OF ϕ VS. a/t

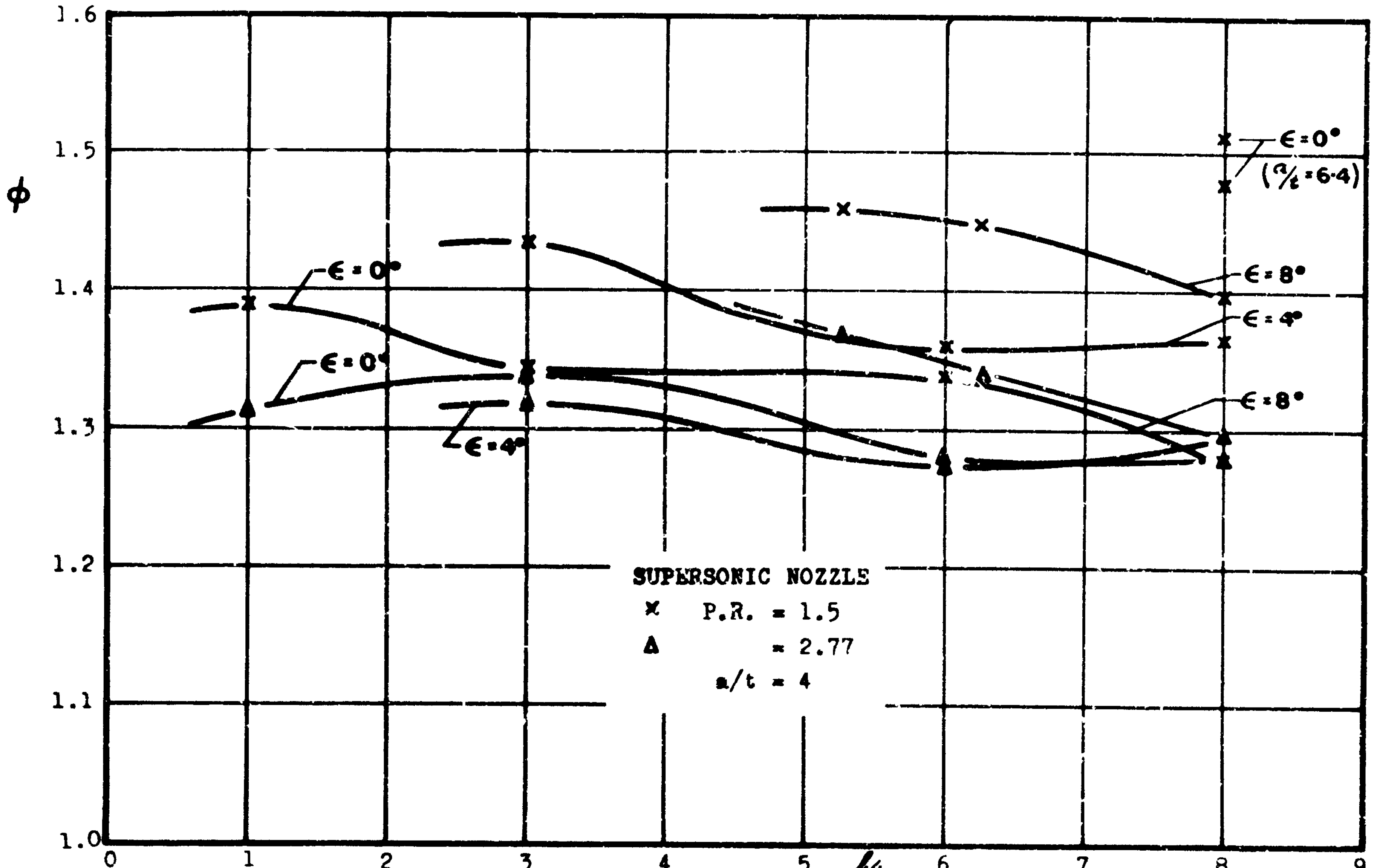


FIG. 19 PLOT OF ϕ VS. ℓ/t FOR VARIOUS VALUES OF ϵ

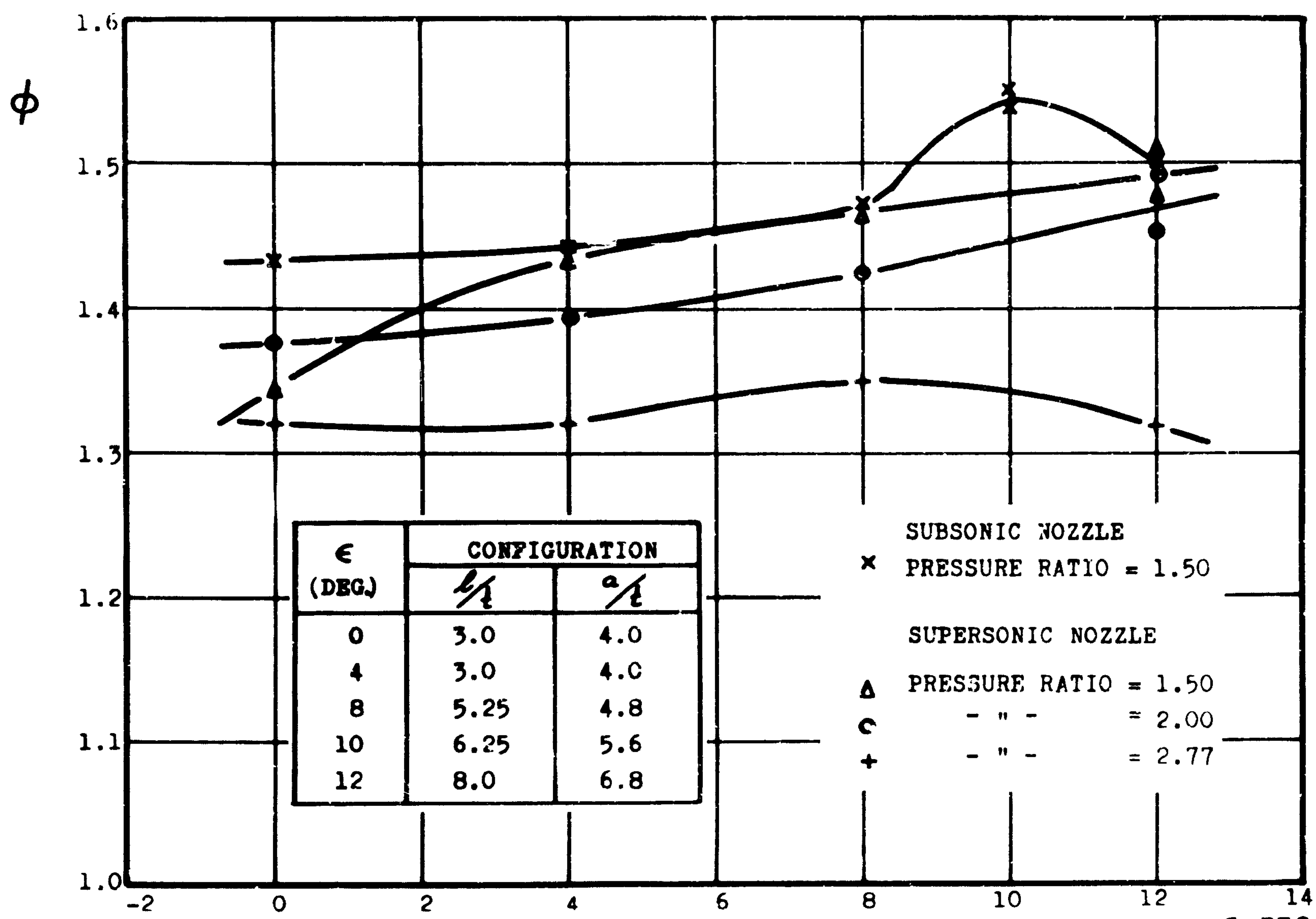


FIG. 20 PLOT OF ϕ VS. ϵ FOR VARIOUS PRESSURE RATIOS

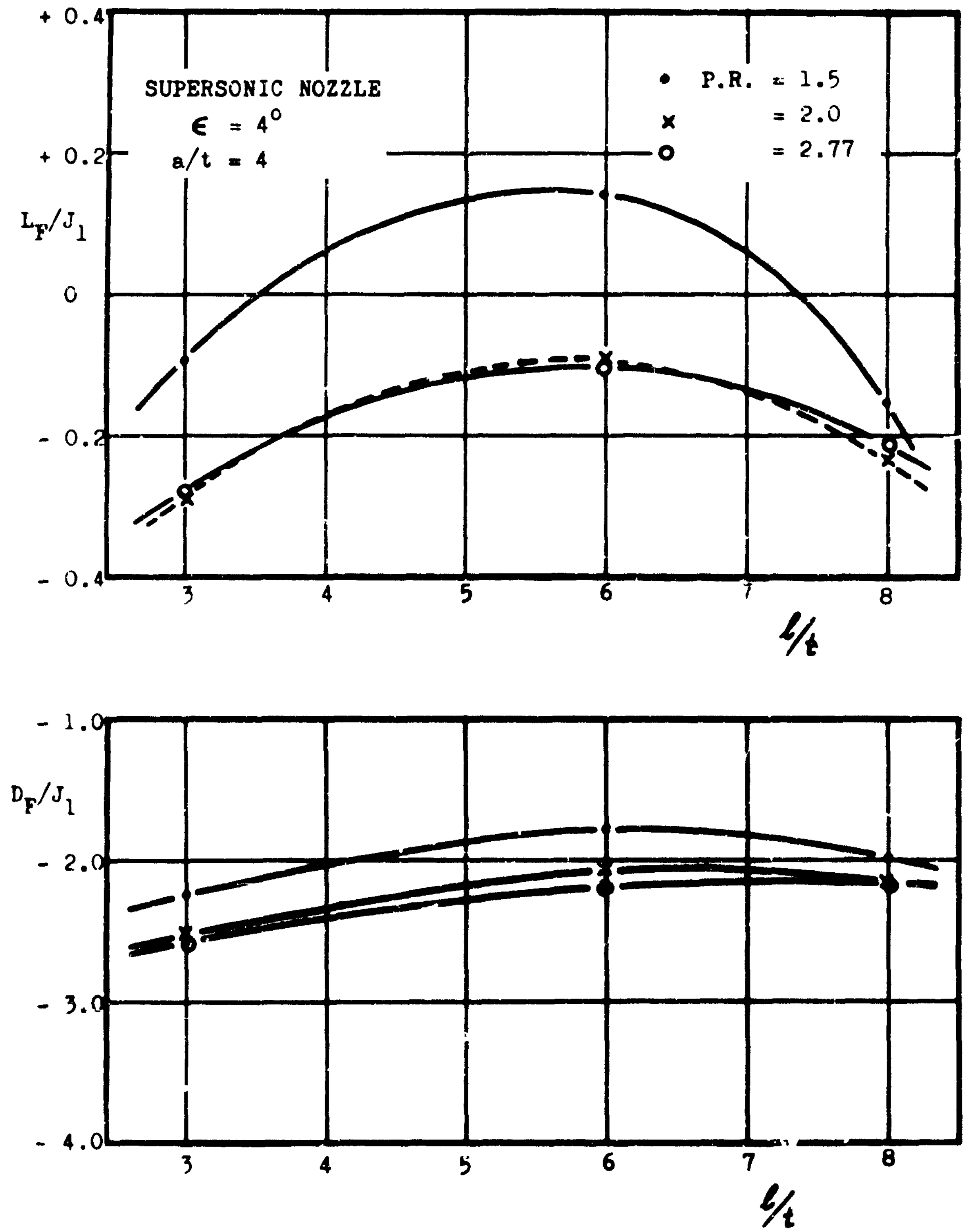


FIG. 21 PLOT OF L_F/J_1 AND D_F/J_1 VS. ℓ/t FOR VARIOUS PRESSURE RATIOS

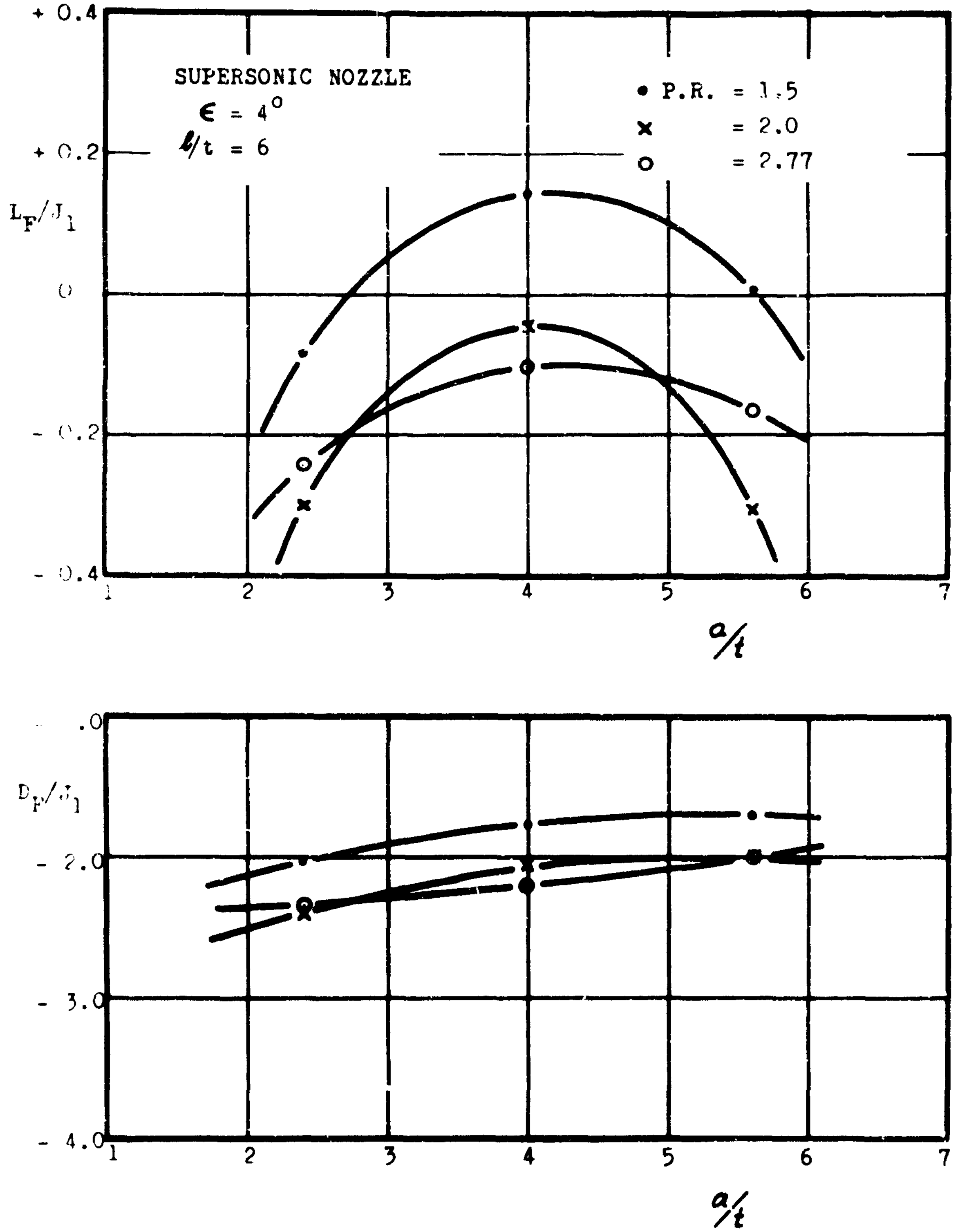


FIG. 22 PLOT OF L_F/J_1 AND D_F/J_1 VS. a/t FOR VARIOUS PRESSURE RATIOS

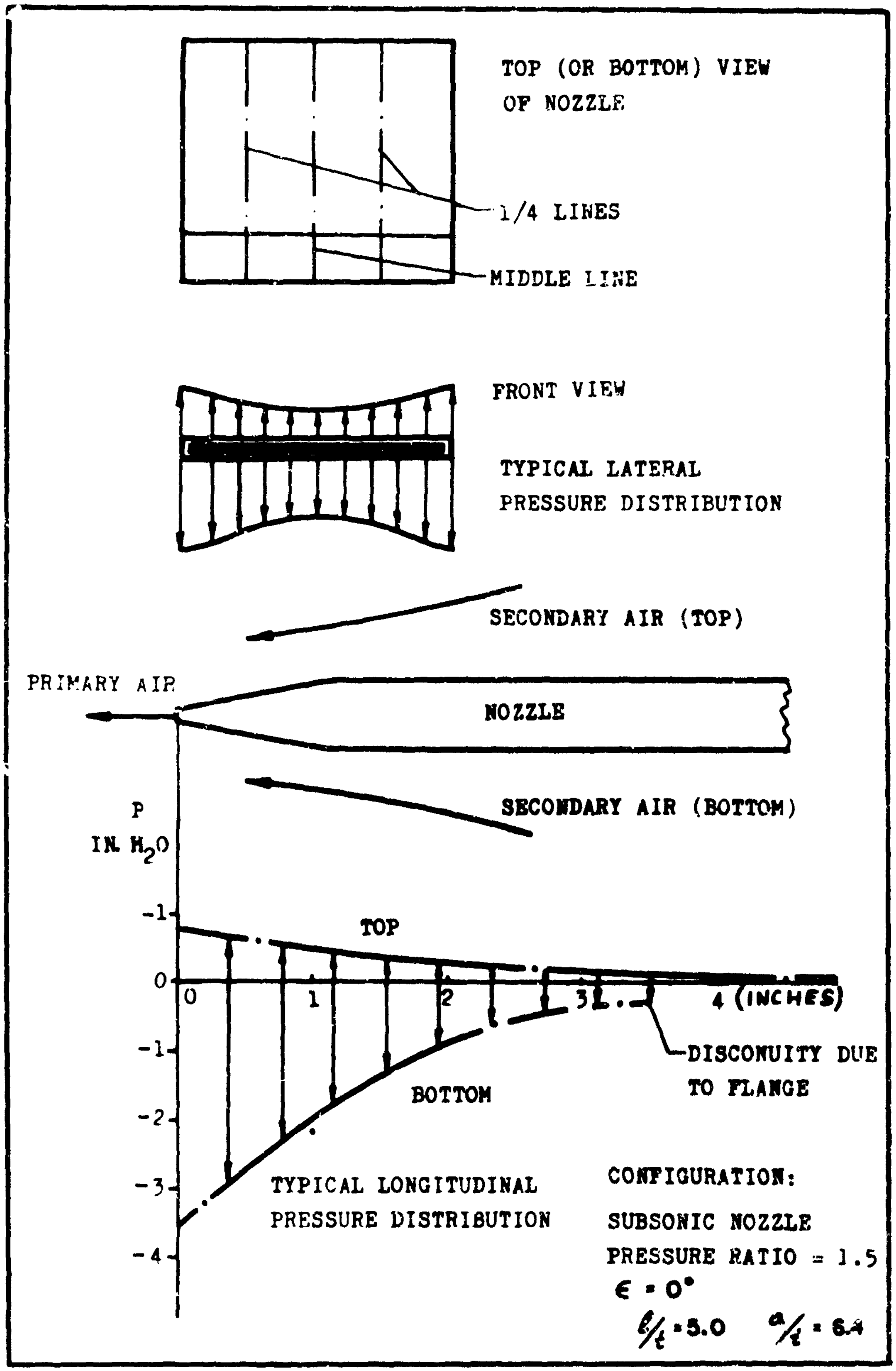


FIG. 23 FLOW AROUND THE NOZZLE

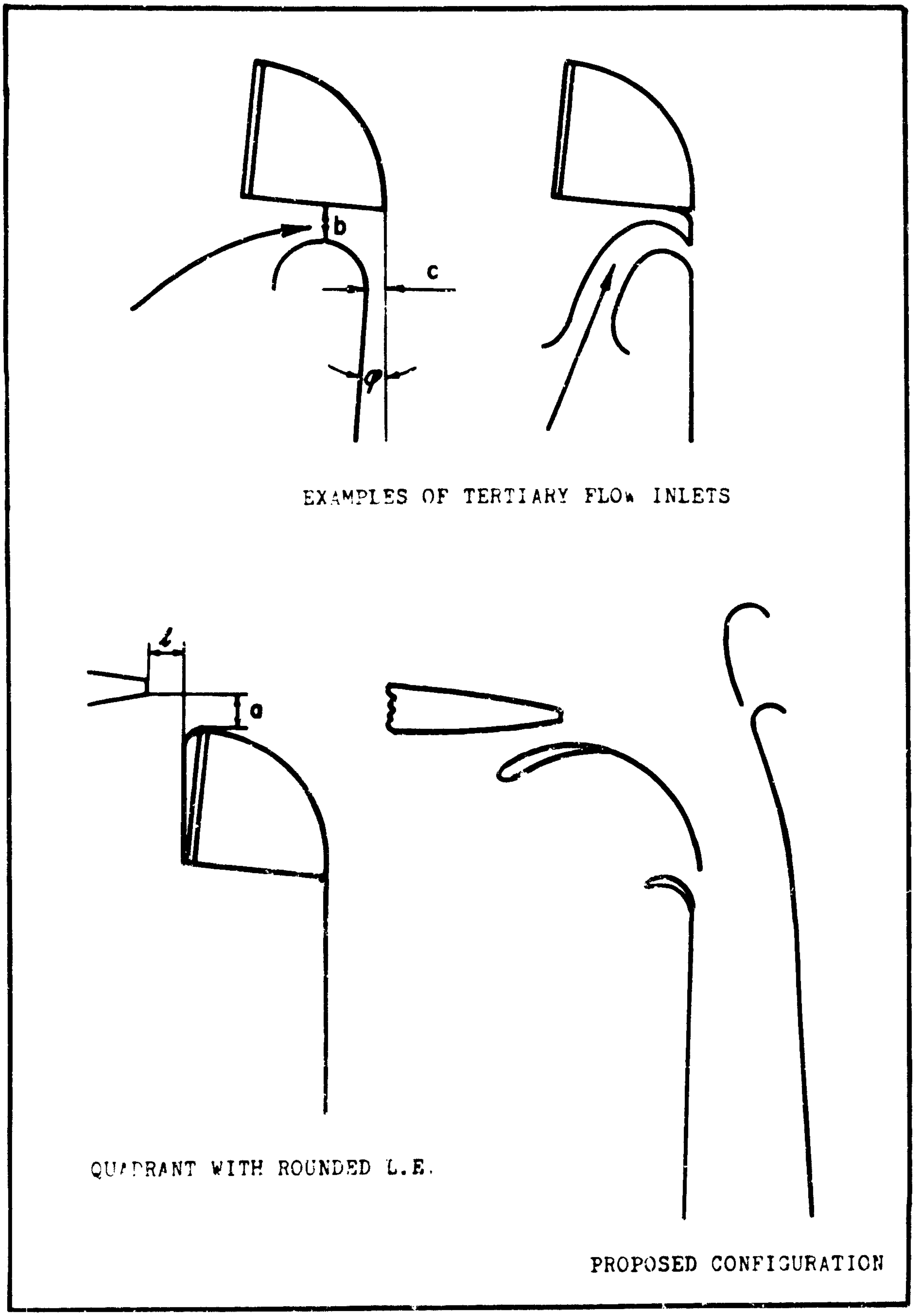


FIG. 24 VARIOUS CONFIGURATIONS

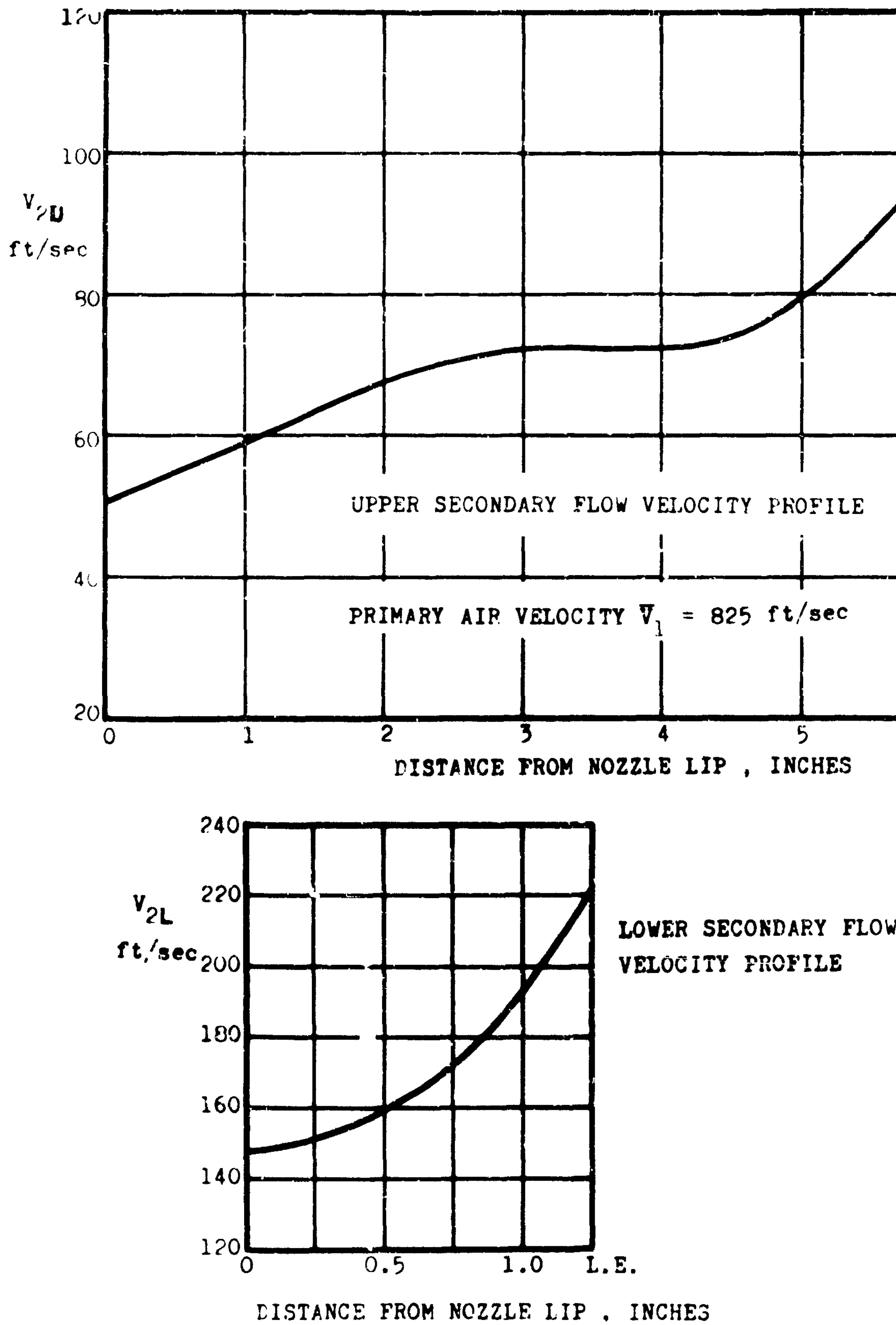


FIG.25 SECONDARY FLOW VELOCITY PROFILES

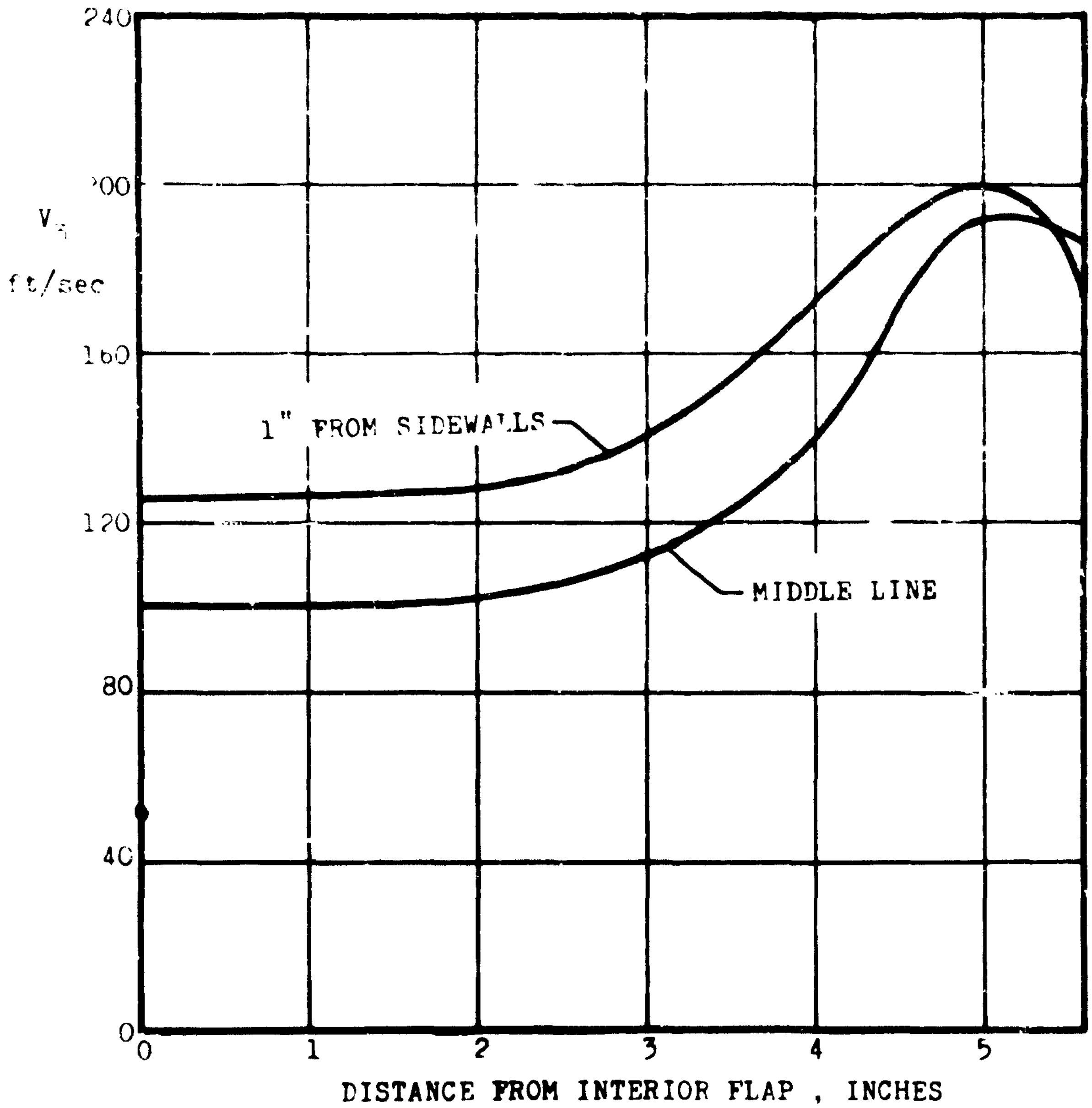


FIG. 26 EXIT MIXED FLOW VELOCITY PROFILE

UTIAS TECHNICAL NOTE NO. 79

Institute for Aerospace Studies, University of Toronto

An Experimental Investigation into the Shape of Thrust Augmenting Surfaces in Conjunction with Coanda-Deflected Jet Sheets (Part II)

T. Mehus   January, 1965   30 pages   26 figures   2 tables

1. Thrust Augmentation   2. Coanda Effect
3. Ground Effect Machines   4. V/STOL Aircraft
I. Mehus, T.   II. UTIAS Technical Note No. 79

The present work is a continuation of the experimental investigations described in Part I. The subject was to increase the thrust augmentation of a configuration consisting of a Coanda surface (quadrant), deflecting the primary jet sheet through 90°, in conjunction with additional (thrust augmenting) surfaces. The effect of a horizontal and vertical gap between the lip of the nozzle and the leading edge of the deflection surface, as well as the effect of a gap between its trailing edge and the downstream diffuser wall (tertiary flow) was studied. These experiments were carried out for a convergent (subsonic) and a convergent-divergent (supersonic) nozzle at various pressure ratios. The subsonic jet sheet produced the highest thrust augmentation. Tilting of the quadrant led to an increase in the augmentation ratio (excluding the lift acting on the nozzle), while the total thrust augmentation (including the lift over the nozzle), did not increase. Typical secondary and exit mixed flow velocity profiles were obtained. The highest total thrust augmentation observed was 1.37.

Available copies of this report are limited. Return this card to UTIAS, if you require a copy.

UTIAS TECHNICAL NOTE NO. 79

Institute for Aerospace Studies, University of Toronto

An Experimental Investigation into the Shape of Thrust Augmenting Surfaces in Conjunction with Coanda-Deflected Jet Sheets (Part II)

T. Mehus   January, 1965   30 pages   26 figures   2 tables

1. Thrust Augmentation   2. Coanda Effect
3. Ground Effect Machines   4. V/STOL Aircraft
I. Mehus, T.   II. UTIAS Technical Note No. 79

The present work is a continuation of the experimental investigations described in Part I. The subject was to increase the thrust augmentation of a configuration consisting of a Coanda surface (quadrant), deflecting the primary jet sheet through 90°, in conjunction with additional (thrust augmenting) surfaces. The effect of a horizontal and vertical gap between the lip of the nozzle and the leading edge of the deflection surface, as well as the effect of a gap between its trailing edge and the downstream diffuser wall (tertiary flow) was studied. These experiments were carried out for a convergent (subsonic) and a convergent-divergent (supersonic) nozzle at various pressure ratios. The subsonic jet sheet produced the highest thrust augmentation. Tilting of the quadrant led to an increase in the augmentation ratio (excluding the lift acting on the nozzle), while the total thrust augmentation (including the lift over the nozzle), did not increase. Typical secondary and exit mixed flow velocity profiles were obtained. The highest total thrust augmentation observed was 1.37.

Available copies of this report are limited. Return this card to UTIAS, if you require a copy.

UTIAS TECHNICAL NOTE NO. 79

Institute for Aerospace Studies, University of Toronto

An Experimental Investigation into the Shape of Thrust Augmenting Surfaces in Conjunction with Coanda-Deflected Jet Sheets (Part II)

T. Mehus   January, 1965   30 pages   26 figures   2 tables

1. Thrust Augmentation   2. Coanda Effect
3. Ground Effect Machines   4. V/STOL Aircraft
I. Mehus, T.   II. UTIAS Technical Note No. 79

The present work is a continuation of the experimental investigations described in Part I. The subject was to increase the thrust augmentation of a configuration consisting of a Coanda surface (quadrant), deflecting the primary jet sheet through 90°, in conjunction with additional (thrust augmenting) surfaces. The effect of a horizontal and vertical gap between the lip of the nozzle and the leading edge of the deflection surface, as well as the effect of a gap between its trailing edge and the downstream diffuser wall (tertiary flow) was studied. These experiments were carried out for a convergent (subsonic) and a convergent-divergent (supersonic) nozzle at various pressure ratios. The subsonic jet sheet produced the highest thrust augmentation. Tilting of the quadrant led to an increase in the augmentation ratio (excluding the lift acting on the nozzle), while the total thrust augmentation (including the lift over the nozzle), did not increase. Typical secondary and exit mixed flow velocity profiles were obtained. The highest total thrust augmentation observed was 1.37.

Available copies of this report are limited. Return this card to UTIAS, if you require a copy.

UTIAS TECHNICAL NOTE NO. 79

Institute for Aerospace Studies, University of Toronto

An Experimental Investigation into the Shape of Thrust Augmenting Surfaces in Conjunction with Coanda-Deflected Jet Sheets (Part II)

T. Mehus   January, 1965   30 pages   26 figures   2 tables

1. Thrust Augmentation   2. Coanda Effect
3. Ground Effect Machines   4. V/STOL Aircraft
I. Mehus, T.   II. UTIAS Technical Note No. 79

The present work is a continuation of the experimental investigations described in Part I. The subject was to increase the thrust augmentation of a configuration consisting of a Coanda surface (quadrant), deflecting the primary jet sheet through 90°, in conjunction with additional (thrust augmenting) surfaces. The effect of a horizontal and vertical gap between the lip of the nozzle and the leading edge of the deflection surface, as well as the effect of a gap between its trailing edge and the downstream diffuser wall (tertiary flow) was studied. These experiments were carried out for a convergent (subsonic) and a convergent-divergent (supersonic) nozzle at various pressure ratios. The subsonic jet sheet produced the highest thrust augmentation. Tilting of the quadrant led to an increase in the augmentation ratio (excluding the lift acting on the nozzle), while the total thrust augmentation (including the lift over the nozzle), did not increase. Typical secondary and exit mixed flow velocity profiles were obtained. The highest total thrust augmentation observed was 1.37.

Available copies of this report are limited. Return this card to UTIAS, if you require a copy.